General Disclaimer

One or more of the Following Statements may affect this Document

- This document has been reproduced from the best copy furnished by the organizational source. It is being released in the interest of making available as much information as possible.

- This document may contain data, which exceeds the sheet parameters. It was furnished in this condition by the organizational source and is the best copy available.

- This document may contain tone-on-tone or color graphs, charts and/or pictures, which have been reproduced in black and white.

- This document is paginated as submitted by the original source.

- Portions of this document are not fully legible due to the historical nature of some of the material. However, it is the best reproduction available from the original submission.

NASA

DEVELOPMENT OF A PLASMA SPRAYED
CERAMIC GAS PATH SEAL FOR
HIGH PRESSURE TURBINE APPLICATIONS

By: L. T. Shiembob and J. F. Hyland

Pratt & Whitney Aircraft Group
Commercial Products Division
United Technologies Corporation

Prepared for

1. Report No.	2. Government Accession No.	3. Recipient's Catalog No.
4. Title and Subtitle Development of a Plasma Sprayed Ceramic Gas Path Seal for High Pressure Turbine Applications		5. Report Date Sept. 1979
		6. Performing Organization Code
7. Author(s) L. T. Shiembob and J.F. Hyland		8. Performing Organization Report No. 5633-11
		10. Work Unit No.
9. Performing Organization Name and Address Pratt & Whitney Aircraft Group Commercial Products Division United Technologies Corporation East Hartford, Connecticut 06108		11. Contract or Grant No. NAS3-21390
12. Sponsoring Agency Name and Address Propulsion Laboratory U.S. Army R&T Labs (AVRADCOM) Lewis Research Center Cleveland, Ohio 44135		13. Type of Report and Period Covered Contractor Report 9/12/78 - 4/12/79
		14. Sponsoring Agency Code

15. Supplementary Notes

Project Manager, Dr. Robert C. Bill
NASA Lewis Research Center
Cleveland, Ohio 44135

16. Abstract

Development of the plasma sprayed graded, layered ZrO_2/CoCrAlY seal system for gas turbine engine blade tip seal application up to $1589°K$ $(2400°F)$ surface temperature reported in NASA reports CR-135183 and CR-135387 was continued. Methods of improvement of the cyclic thermal shock resistance of the sprayed zirconia seal system were investigated. The most promising method, reduction of the ceramic thickness and metallic substrate stiffness were selected based upon potential and feasibility. Specimens were fabricated and experimentally evaluated to 1) substantiate the capacity of the geometry changes to reduce operating stresses in the sprayed structure and 2) define the abradability, erosion, thermal shock and physical property characteristic for the sprayed ceramic seal system. Thermal stress analysis was performed and correlated with thermal shock test results.

Results of the analysis and testing indicates that the geometry modifications succeeded in improving the thermal shock capabilities of the system. Abradability, erosion and physical properties of the modified system remained basically unchanged. Analysis of an alternate system indicated that even more thermal shock capability can be achieved with further geometry modifications.

| 17. Key Words (Suggested by Author(s))
Seal, Abradable
Seal, Turbine
Seal, Blade Tip
Seal, Gas Path
Seal, Plasma sprayed   (continued on page ii) | 18. Distribution Statement | |
| 19. Security Classif. (of this report)

Unclassified | 20. Security Classif. (of this page)

Unclassified | 21. No. of Pages | 22. Price* |

NASA-C-168 (Rev. 10-75)

1.0 SUMMARY

The program to improve the cyclic thermal shock resistance of the
sprayed Zirconia seal system evaluated under NAS3-20623 continued with
an analytical investigation of the effects of residual stress manage-
ment and geometry modifications. A design with modified geometry, name-
ly, reduced ceramic and substrate thickness and slotted rails, was
selected for fabrication and experimental evaluation.

Simulated engine cycle thermal shock rig testing indicated that the
geometry modifications did reduce crack severity and propagation al-
though both the baseline and improved geometry specimens showed more
sensitivity to the thermal environment than the baseline configuration
specimen tested earlier and described in NASA report CR-135387. It is
possible, as explained later in this report, that stresses generated
during machining may have weakened the test specimens and made them
more susceptible to thermally induced stresses.

The analysis of both the improved geometry and baseline systems corre-
lated extremely well with the actual thermal shock test results. The
maximum stress-to-strength value for both systems occurred at the point
of actual crack initiation during the acceleration transient from idle
to sea level take off. In addition crack progression during other
points of the complete thermal cycle corresponded with the location of
maximum stress to strength ratios.

Refined measurement techniques and improved fixturing resulted in more
accurate definition of the system properties. The use of the refined
properties in the thermal analysis contributed to the good correlation
between the analysis and thermal shock test results.

Erosion resistance of the baseline and improved geometry specimens was
basically identical and unchanged from previous tests under NAS3-19759
and NAS3-20623.

Abradability test results of baseline and improved geometry were not
conclusive in that 50 percent of the specimens spalled prior to comple-
tion of the tests. Cracks generated during machining contributed to
these spallations. A review of rig test data, however, indicated rub
performance of both systems to be basically consistent with previous
testing reported in NASA CR-134579, CR-135183 and CR-135387.

Additional analysis to determine an alternative system indicated that
1.143 mm (.045 in) thick ZrO_2 version of the improved geometry system
would be expected to have significantly improved thermal shock charac-
teristics. The maximum stress to strength ratio at all operating condi-
tions was calculated to be less than 1.0. Test specimens for this
system have been fabricated.

2.0 INTRODUCTION

2.1 Previous Contractual Experience

The program to develop a plasma sprayed graded yttria stabilized cera-
mic (zirconia)/metal (CoCrAlY) seal system for turbine blade tip seal
application reported in NASA CR-134879, CR-135183 and CR-135387 has
produced encouraging results. Initial effort defined a baseline confi-
guration composed of a ceramic top layer and three intermediate mixed
layers of zirconia and CoCrAlY. Ceramic concentrations in these layers,
progressing from the substrate to the ceramic layer, were 40, 70, and
85 percent, respectively. This initial configuration demonstrated pro-
mising abradability and erosion resistance, but the ability of the seal
to withstand thermal shock and fatigue remained a concern.

To evaluate the thermal shock and fatigue capabilities of the seal sys-
tem, the physical properties of each of the graded layers were defined
experimentally and used in a thermal and stress analysis using a typi-
cal engine thermal cycle. The results of this analysis confirmed the
need for further development indicating that the tensile stresses in
the ceramic layer caused by thermal conditions would exceed the
strength of the ceramic at the surface during the engine thermal cycle.
On this basis, it was concluded that radial cracks would occur in the
central portion of the ceramic surface as a result of thermal strain.

A seal specimen was subsequently subjected to thermal fatigue tests
simulating the conditions used in the analysis. The results confirmed
the analysis; radial cracks were produced in the center of the ceramic
surface. However, laminar cracking, not predicted by the analysis, also
occurred. Several possible causes for the laminar cracking were identi-
fied. Subsequent thermal and stress analysis indicated the benefit of
reducing the number of intermediate layers from three to two with
ceramic-to-metallic ratios of 40/60 percent and 85/15 percent. This
approach simplified the fabrication process with no increase in pre-
dicted stress. Testing of this configuration demonstrated a capability
to withstand 100 simulated engine thermal cycles without spalling.

Various other approaches were investigated in an attempt to further
improve the system's ability to withstand thermal shock and fatigue.
Included were changes in the material composition of the layers, pre-
straining the seal by mechanical and thermal treatment of the substrate
prior to spraying, annealing following spraying, and changing the
geometry of the substrate.

Analysis of the potential effects of varying the material composition
indicated that the intermediate zirconia-metal layer ratios are approx-
imately optimum with respect to minimizing thermal stresses. Only
slight improvement could be obtained by this approach, but the improve-
ment would not be sufficient to reduce the maximum stress below the
measured material strength. Hence, this approach could not, by itself,
provide the full solution to the problem.

Analyses indicated the possibility of utilizing mechanical pre-stress to reduce thermal stress in the system during engine operation. This approach was not considered for evaluation, however, because of the complexity and cost associated with the design and fabrication of suitable fabrication fixtures.

Post spray annealing was not considered feasible because rupture stresses would be induced at the 40/60 ZrO_2/CoCrAlY layer at temperatures well below the temperature at which reasonable creep rates would occur in the metal substrate.

Thermal prestraining of the metal substrate was found to offer the most potential for inducing compressive residual stresses in the seal system and was further evaluated through both testing and analysis.

The analyses indicated that heating the substrate to 922°K (1200°F) prior to and during spraying would introduce residual compressive stresses that would reduce the tensile stresses in the center of the seal system during thermal cycling. Analysis based on information available at the time, however, indicated that the effect near the edges would be small, and the maximum tensile stress that would be experienced during thermal cycling would still exceed the strength in the ZrO_2 and the 85/15 ZrO_2/CoCrAlY layers. Laminar cracking or delamination at the edges, seen in subsequent thermal shock rig testing, substantiated these findings. Other properties of the ceramic system were unchanged by heating the substrate. Abradability and erosion characteristics were shown to be virtually unaffected. Erosion testing did show a slight tendency toward improved erosion resistance, but data generated to date is not sufficient to be conclusive.

The NAS3-20623 baseline system fabricated without supplemental heating was also tested in the cyclic thermal shock rig for comparative purposes and successfully completed 500 cycles without spalling.

2.2 Current Program Overview

The objective of this program was to continue the development of the sprayed graded zirconia/CoCrAlY system for use as a turbine blade tip seal. Specifically, two approaches were investigated to reduce the tensile stresses predicted to result from engine thermal cycling while maintaining or improving both abradability and erosion resistance. The two approaches were: 1) reduce thermal stresses by modifying the geometry and structure of the system and 2) application of residual stress management. Both approaches were analyzed and evaluated, and the best approach, a geometry modification which involved a reduction in the stiffness of the substrate was selected for evaluation.

Parts were fabricated by spraying the ceramic on both the baseline and improved geometry substrates. Physical property data was determined, tests conducted, and test results correlated with analysis and previous data. Recommendations for further development were formulated. In addition, further analysis identified the benefit, in terms of stress reduction, associated with further reducing the ZrO_2 layer thickness. Parts of this alternate design were fabricated for future evaluation.

3.0 TECHNICAL PROGRAM

3.1 Analysis

Baseline configuration parts, shown schematically in Figure 1, fabricated without supplemental heating of substrate and with substrates at $922^{\circ}K$ ($1200^{\circ}F$) during spray deposition were exposed to a typical engine thermal cycle in the cyclic thermal shock rig, Figure 2, and the results reported in NASA CR-135387. An analysis was conducted on both parts to estimate the thermal stresses generated during the rig test. This analysis utilized latest available physical properties and residual stress data to investigate the correlation between both stress-to-strength ratio and strain to strain to failure ratio and crack initiation during rig test. The analyses focused on the circumferential configuration which historically has been limiting with respect to thermal stresses. Acceleration, sea level take off (SLTO) and deceleration operating cycles were investigated. The results of this evaluation are presented in Figures 3 through 6.
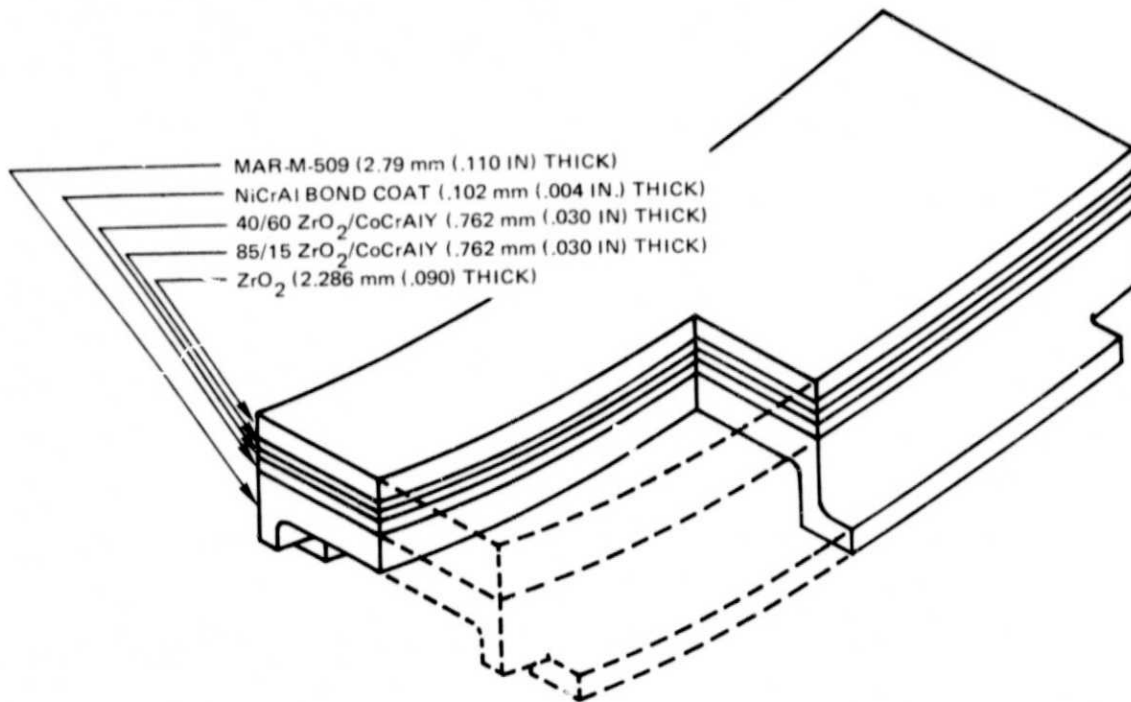

MAR-M-509 (2.79 mm (.110 IN) THICK)
NiCrAl BOND COAT (.102 mm (.004 IN.) THICK)
40/60 ZrO_2/CoCrAlY (.762 mm (.030 IN) THICK)
85/15 ZrO_2/CoCrAlY (.762 mm (.030 IN) THICK)
ZrO_2 (2.286 mm (.090) THICK)

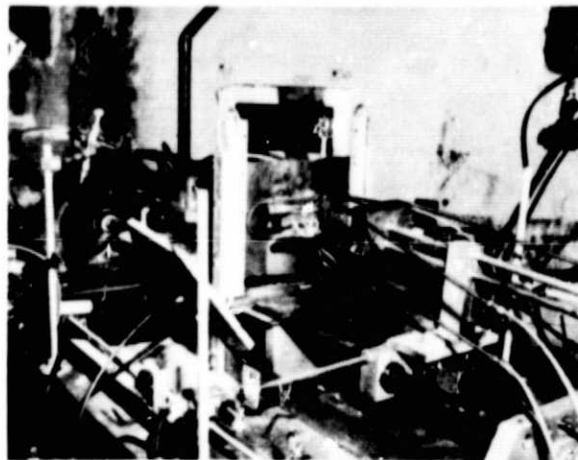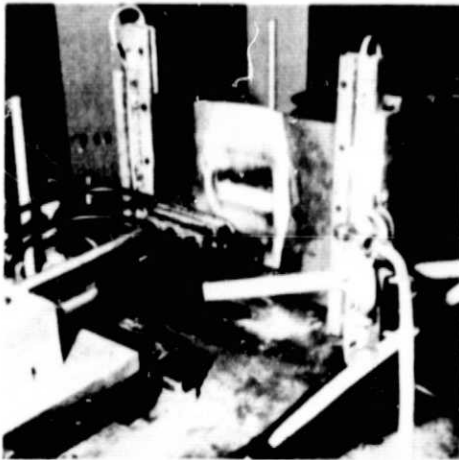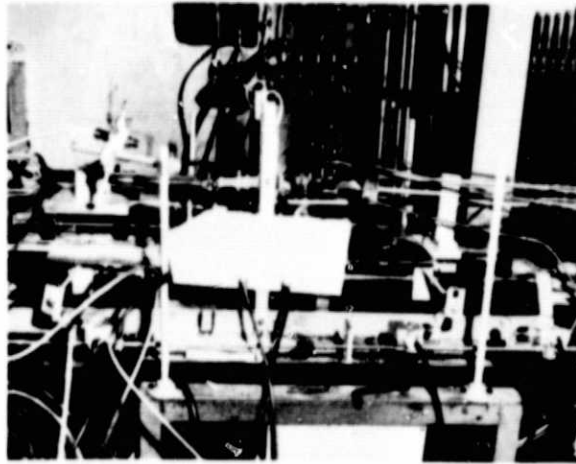Figure 1   Typical Abradability Specimen

4

Figure 2   Cyclic Thermal Shock Test Rig

The results of the analysis of the parts employing the $922^\circ K$ ($1200^\circ F$) preheated substrate during spray deposition correlated favorably with the actual test results. Stress-to-strength and strain to strain to failure ratios shown in Figure 3 are maximum and of sufficient magnitude, greater than 1.0, to indicate crack initiation at the edge of the part at the ZrO_2-85/15 ZrO_2/CoCrAlY interface during the acceleration portion of cycle. Crack initiation actually occurred during test at this location during the acceleration transient. The crack location is shown as well as the location of maximum stress-to-strength and strain-to-failure ratios in Figure 4.

The thermal stresses during deceleration and the 40/60 ZrO_2/CoCrAlY layer acceleration and SLTO stresses were not shown in Figures 3 and 4 because they were insignificant in magnitude.
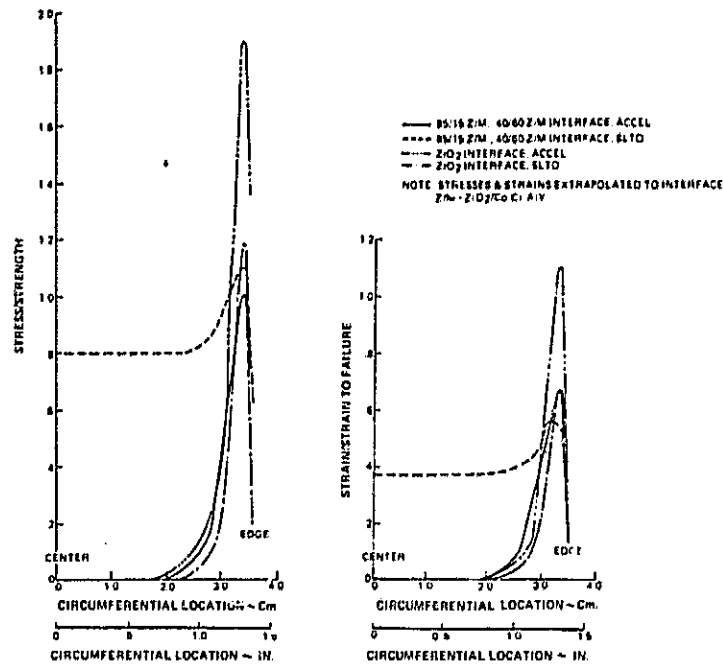
Figure 3   Stress/Strength and Strain/Strain to Failure Ratios for the 922°K (1200°F) System Predicts Failure at the ZrO_2 Interface, near the Edge during Acceleration
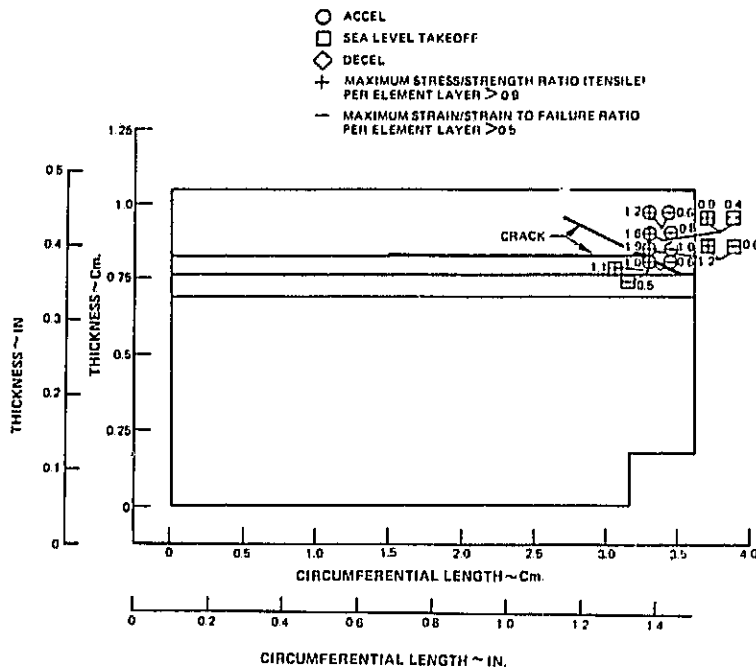
Figure 4   Maximum Stress/Strength & Strain/Strain to Failures Ratios for 922°K (1200°F) System Occurs at Crack Location
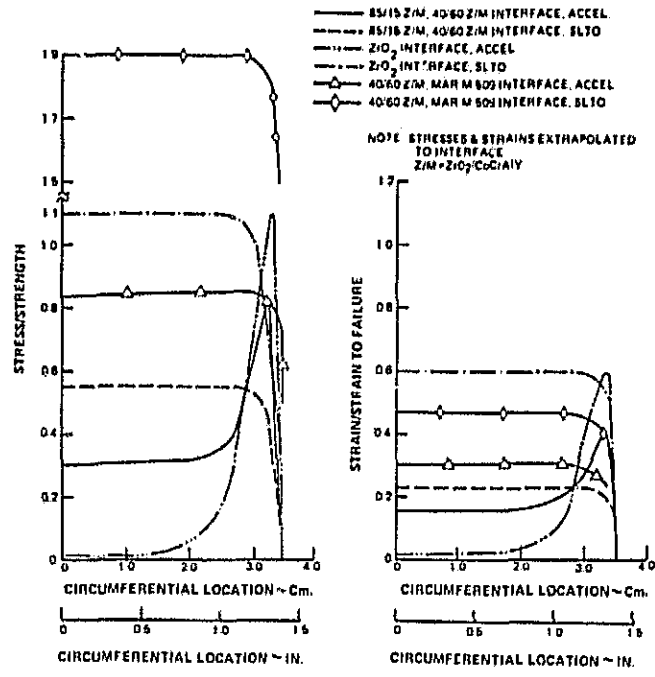
6

Figure 5   Stress/Strength Ratios for the Baseline System Predict
            Failure at the ZrO_2 Interface Near the Edge During
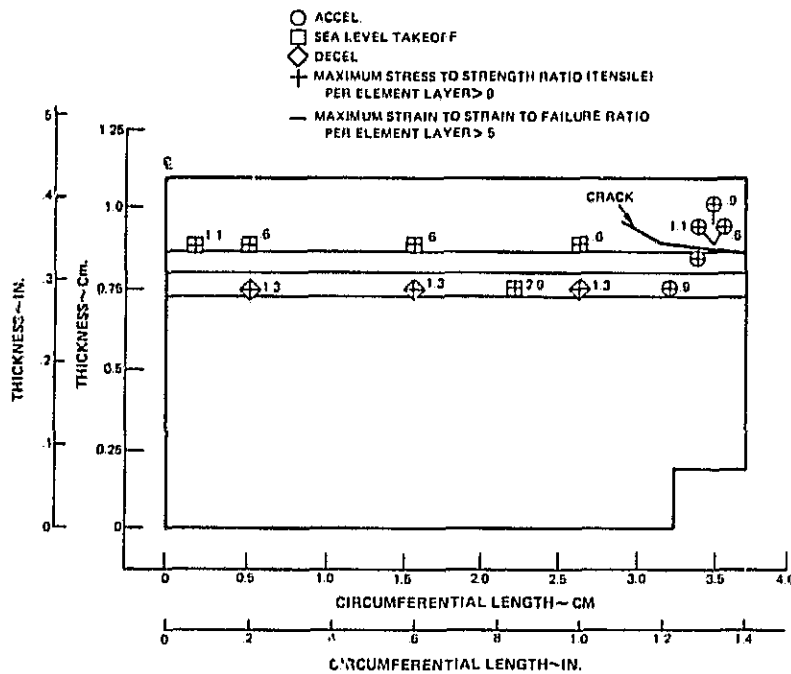   Acceleration

Figure 6   Maximum Stress/Strength Ratio in the ZrO_2 Layer for the
            Baseline System Occurs at the Crack Location During
            Acceleration

The results of the baseline system analyses did not produce the same correlation with the actual test results. The maximum estimated stress-to-strength ratio (1.9) shown in Figure 5 was calculated to occur during deceleration at the 40/60 ZrO_2/CoCrAlY substrate interface and the maximum strain to strain-to-failure ratio (.6) was not sufficient to indicate crack intiation. The result of the thermal shock test of the baseline system is shown in Figure 6 with the more important analytically predicted stress-to-strength and strain to strain to failure values. Crack initiation occurred at the ZrO_2 - 85/15 ZrO_2/CoCrAlY interface after 100 cycles.

Subsequent experimental and analytical effort described later in this report indicates that the correlation between analyses and test results might have been improved by more complete property data.

3.2   Improved System Selection

Testing as reported in NASA CR-135183 and CR-135387 indicated that the thermal stresses produced in the seal system during engine operating conditions must be reduced. Several approaches were investigated on a preliminary basis and indicated sufficient potential for further investigation. As a result, an analytical study was conducted to investigate the possibility of reducing thermal stress by 1) modification to the geometry of the configuration and 2) residual stress management.

Various geometry modifications were investigated analytically to determine which modification or combination offered the greatest potential to reduce thermal stresses during engine operation. The analyses utilized latest available property data and the residual stress distribution defined under a current NASA contract NAS3-20590. The analytical program to define the stresses generated during engine operation required that the residual stresses be incorporated by developing an associated stress free temperature (SFT) distribution. The SFT is the temperature distribution at which the part is stress free and is used to calculate stresses by means of the difference between the operating temperature and the SFT. The stresses calculated at room temperature would, for example, utilize the difference between room temperature and the SFT and associated property/temperature relationship and define the residual stress of the part. The circumferential configuration at acceleration conditions, generally the greatest stress condition, was used in the analysis.

Previous analysis of the effect of geometric modification on thermal stress as reported in NASA CR-135183 and CR-13587 considered the number and thickness of intermediate layers and the ratio of metallic and ceramic in the intermediate layers. The current configuration was a result of these analyses and further effort to optimize these features was not considered worthwhile. Geometry modifications that were considered in this analysis were 1) reducing the ZrO_2 thickness, 2) reducing substrate thickness and 3) reducing the stiffness of the substrate by slotting the substrate rails.

8

The geometric configurations that were analyzed are shown in Table 1. The slotted rail configuration considered was 13 equally spaced machining cuts .762 to 1.016mm (.030 to .040 in) thick.

Table 1

Geometry Configurations of Several Alternatives
Investigated Analytically

| | Baseline | Alternatives | | | | | |
		1	2	3*	4	5	6
ZrO_2 Thickness ~ cm	.2286	.2286	.1524	.1524	.1524	.1524	.1524
85/15 ZrO_2/CoCrAlY Thickness~cm	.0762	.0762	.0762	.0762	.0762	.0762	.0762
40/60 ZrO_2/CoCrAlY Thickness ~ cm	.0762	.0762	.0762	.0762	.0762	.0762	.0762
Substrate Thickness ~ cm	.2794	.2794	.2794	.1524	.1524	.1524	.1524
Rail Configuration	Solid	Slotted (13)	Slotted (13)	Slotted (13)	Slotted (13)	Slotted (13)	Slotted (13)
Stress Free Temperature Distribution °K (°F)	NAS3-20590 Baseline	NAS3-20590 Baseline	NAS3-20590 Baseline	NAS3-20590 Baseline	Constant 700 (800)	Constant 811 (1000)	Constant 922 (1200)

* Selected Improved Geometry System

Analysis was also conducted to evaluate the effect of residual stress management. Although the program did not provide for effort to define the fabrication process required to produce a given residual stress distribution, the analysis attempted to evaluate the potential effect on operating stresses associated with residual stress management. Specifically, cases were analyzed in which the configuration offering the lowest thermal stresses was evaluated with residual stress equivalent to a constant stress free temperature (SFT) of 700°K (800°F), 811°K (1000°F), and 922°K (1200°F) - alternatives 4-6 on Table 1.

Results of the analyses indicated that of the three geometric configuration changes considered, the greatest reduction in thermal stresses would be achieved by alternative 3, that is, by reducing the substrate and ZrO_2 thickness and reducing the stiffness of the support rails. This configuration was then used to determine any additional benefit in terms of stress free temperature that could be acquired by managing residual stresses. Table 2 presents the results of the analysis. The maximum stress to strength ratio during the accel transient in the ZrO_2 at the 85/15 ZrO_2/CoCrAlY interface, the 85/15 ZrO_2/CoCrAlY at the 85/15 ZrO_2/CoCrAlY -40/60 ZrO_2/CoCrAlY interface and in the 40/60 ZrO_2/CoCrAlY at the 40/60 ZrO_2/CoCrAlY - substrate interface is presented.

Table No. 2

Comparison of Stress/Strength Ratios Indicate The Benefit of The Improved Geometry System

Row	Case	Stress to Strength Ratio		
		ZrO₂-85/15 Z/H Interface	85/15 Z/H-40/60 Z/H Interface	40/60 Z/H-Substrate
1	Baseline Accel	1.15	0.78	0.41
2	Slotted Rails Accel Alternative No. 1	1.08	0.65	0.44
3	Slotted Rails .060 ZrO₂ Accel Alternative No. 2	0.86	0.68	0.46
4	Improved Geometry Accel Alternative No. 3	0.76	0.51	0.46
5	922°K Improved Geometry Accel Alternative No. 6	0.92	1.14	0.45
6	811°K Improved Geometry Accel Alternative No. 5	0.96	1.31	0.43
7	700°K Improved Geometry Accel Alternative No. 4	1.00	1.45	0.41
8	Baseline SLTO	1.30	0.41	0.63
9	Improved Geometry System SLTO Alternative No. 3	0.97	0.33	0.64
10	922°K Improved Geometry SLTO Alternative No. 6	0.46	1.09	0.18
11	Baseline Decel	0.41	0.15	0.23
12	Improved Geometry System Decel Alternative No. 3	0.37	0.08	0.20

Results, noted in the first four rows, indicate the benefit of reducing substrate thickness and reducing rail stiffness by the reduction of the stresses in the ZrO_2 to 0.76. The lack of similar benefit in the 40/60 ZrO_2/CoCrAlY layer was not considered significant in that the magnitude of stress to strength ratio was well below 1.

Results of analysis at the acceleration condition of alternative stress free temperatures of 922°K (1200°F), 811°K (1000°F) and 700°K (800°F), shown in Rows 5-7 did not indicate additional benefit. The best alternative, a constant 922°K (1200°F) stress free temperature, was shown to have additional benefit at the SLTO condition, Row 10, in reducing stresses in the ZrO_2 but at a cost of increasing the stresses in the 85/15 ZrO_2/CoCrAlY layer to a value greater than the layer strength by 9%. On the basis of this data, the improved geometry, consisting of reduced substrate thickness and reduced rail stiffness without residual stress control was evaluated. A final analytical check was conducted to insure that stresses during the decel transient would be acceptable. Results, shown in the last row of Table 2 indicate stresses comparable or less than the baseline configuration.

3.3 Seal System Evaluation

The capability of the improved geometry system was evaluated by rig testing and analysis and compared with the baseline configuration performance. Parts of both the baseline and improved geomr..ry system were fabricated and subjected to abradability, erosion and cyclic thermal shock rig testing. Properties were measured and thermal stress analysis was conducted to evaluate the stresses generated during cyclic thermal shock rig testing and correlate analytical results with crack initiation and progression during rig test.

3.3.1 Fabrication

Three types of substrates were fabricated; 1) Mar-M-509 castings of the configurations shown in Figure 1, 2) Flats of Hastelloy X, and 3) Flats of low alloy steel. The castings were used to fabricate specimens for cyclic thermal shock and abradability testing. The Hastelloy X flats were used to fabricate erosion specimens. The low alloy steel flats were used to fabricate material property specimens. All the substrates were approximately 2.794mm (.110 in) thick except the improved geometry system parts which were 1.524mm (.060 in) thick. The improved geometry system castings for cyclic thermal shock and abradability testing also had 13 equally spaced slots approximately .762mm (.030 in) wide machined into the rails.

All spec: ehi except the material property specimens were sprayed with 4 distinct layers, 1) NiCrAl base coat (approximately .102mm (.004 in) thick), 2) 40/60 ZrO_2/CoCrAlY (approximately .762mm (.030 in) thick) and ZrO_2 3.048mm (.120 in) thick). The material property specimens were sprayed with 2 distinct layers, 1) NiCrAl bond coat (approximately .102mm (.004 in) thick) and 2) a 3.175mm (.125 in) thick ceramic layer.

All of the specimens were final machined after plasma spraying. Laminar cracks near the 85/15 ZrO_2/CoCrAl -40/60 ZrO_2/CoCrAlY interface were generated during final machining in all of the improved geometry system parts.

An investigation of the machining techniques and procedures was conducted. Results of the investigation indicated that the method of fixturing the parts during machining may have been responsible. The fixture provided support for only half of the length of the part with the other half cantilevered. It is possible that the load generated on the cantilevered end of the part during machining contributed to the cracking. The cracks were noticeable on the improved geometry part which has less substrate stiffness than the baseline parts. It is possible that the same machining techniques also effected the baseline parts although not as noticeable as the improved geometry parts because of the stiffer substrate.

3.3.2 Rig Testing

Abradability, erosion and thermal shock testing for both the baseline and improved geometry systems were performed. Testing indicated that the improved geometry system had superior thermal shock capabilities and erosion characteristics superior to the baseline.

3.3.2.1 Abradability Test Results

Abradability rig tests were conducted under simulated engine condition of seal surface temperature, blade tip speed and incursion rate.

All abradability tests were performed with P&WA's high temperature abradability test rig shown in Figure 7. Twelve simulated turbine blade tips were mounted in the periphery of a disk driven at the required speed by a compressed air turbine. The seal segment specimen was mounted in a fixture at the end of a horizontal post attached to a movable carriage assembly. The carriage assembly moves the specimen radially into the rotor assembly at the required incursion rate. The seal specimen was heated from both surfaces by an oxygen-jet fuel burner directed at the front surface of the seal and an electric hot air heater directed at the rear surface of the seal. Gas flow, fuel flow and current flow were varied to control the seal surface temperature.
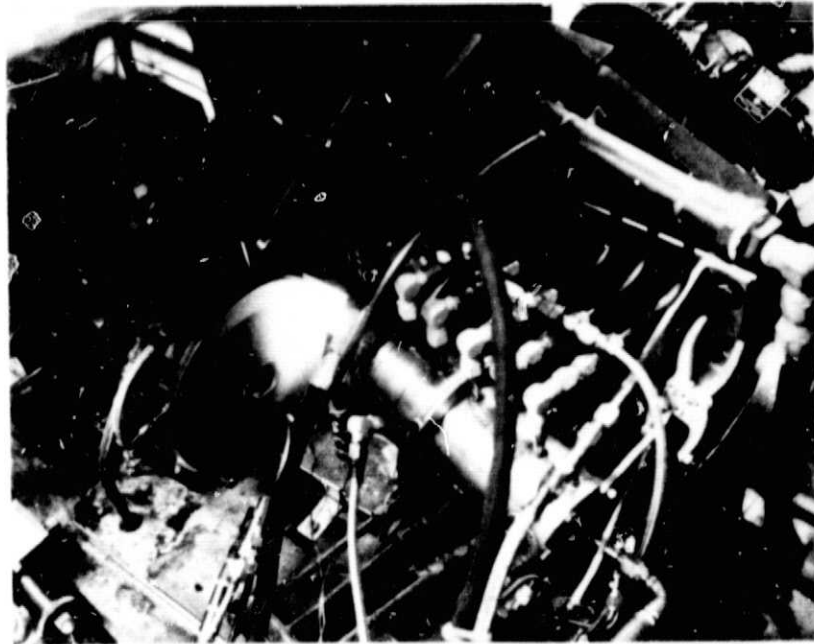

Figure 7   *High Temperature Abradability Test Rig   (PWA-5521)*

Seal surface temperature was monitored by optical pyrometers. Carriage travel was monitored by a linear differential transformer. A load cell in the carriage feed system permitted determination of the average normal force between the seal specimen and blade tips. All data was recorded continuously on a strip chart.

Blade tip and seal wear was determined through pre and post-test measurements. Relative abradability between different specimens and different seal systems was assessed on the basis of the volume wear ratio (VWR): the blade tip wear volume divided by the seal wear volume. The smaller the volume wear ratio, the better the abradability of the seal system.

Four abradability tests were conducted and results are summarized in Ta'le 3 with results of similar testing under previous contracts. The post test conditions of the four parts is shown in Figure 8.

The first test was of a baseline specimen, rubbed at 1589°K (2400°F) surface temperature and 304.8 m/sec (1000 ft/sec) with twelve PWA 1455 blades at an incursion rate of 0.0254 mm/sec (0.001 in/sec). The blades did not groove the seal and the average blade tip wear was 0.909 mm (0.0358 in). Thus a volume wear ratio could not be calculated. A thin layer of blade tip material transfer was evident at the blade contact area.

This result was not consistent with results of earlier testing at this condition of similar systems under (NAS3-19759 and NAS3-20623) which produced as much as .2032 mm (.008 in) of seal wear. All test parameters were checked and determined to be as specified and consistent with previous tests. The average hardness of the ZrO$_2$ surface was measured to be R$_S$45Y 77.3 which is within the range of previously tested specimens. Metallographic inspection also failed to substantiate any significant difference which would explain the difference in abradability.

The second specimen (baseline) was rubbed at the same test conditions except that the incursion rate was 0.254 mm/sec (0.01 in/sec). The blades wore a groove 0.0508 mm (0.002 in) deep in the seal with an average blade tip wear of .5004 mm (0.0197 in), yielding a volume wear ratio of 64.69. This result is consistent with earlier testing. The third and fourth tests were conducted on specimens of the improved geometry. The rig parts developed laminar cracks and spalled severely after approximately 60 percent of the rub interaction.

Spalling that resulted during testing of these specimens is attributed to laminar cracks located at the ends of the part that developed during machining.

Abradability test results could not be compared conclusively with previous data because of lack of seal grooving during the first test at .0254 mm/sec (.001 in/sec) and the lack of complete data on the third and fourth tests because of spalling.

TABLE 3

Abradability Test Summary

| Test No.	NAS3-21390 Test #1	NAS3-21390 Test #2	NAS3-21390 Test #3	NAS3-21390 Test #4	NAS3-20621 Test #1	NAS3-20621 Test #2	NAS3-20621 Test #3	NAS3-20621 Test #4	NAS3-19759 Test #7
Description	Baseline, Machined Surface	Baseline, Machined Surface	Improved Geometry, Machined Surface	Improved Geometry, Machined Surface	922°K(1200°F) System, Machined Surface	Baseline, As-sprayed Surface	922°K(1200°F) System As-sprayed Surface	922°K(1200°F) System As-sprayed Surface	Baseline As-sprayed Surface
Avg. Hardness RS 45Y	77.3	77.3	74.6	-	86.6	74.7	78.0	76.2	70.3
No. Blades	12	12	12	12	12	12	12	12	12
Blade Tip Dia., Cm (in)	21.86(8.61)	21.69(8.54)	21.60(8.50)	21.58(8.50)	21.49(8.46)	21.49(8.46)	21.49(8.46)	21.49(8.46)	21.59(8.5)
Blade Tip Velocity, M/S(Ft/Sec)	304.8(1000)	304.8(1000)	304.8(1000)	304.8(1000)	304.8(1000)	304.8(1000)	284.4(933)	304.8(1000)	304.8(1000)
Seal Temp., °K (°F)	1589(2400)	1589(2400)	1589(2400)	1589(2400)	1589(2400)	1589(2400)	1589(2400)	1589(2400)	1589(2400)
Interaction Rate, MM/S(In/Sec)	0.0254(0.001)	0.2362(0.0093)	0.2286(0.009)	0.0229(0.0009)	-	-	0.0254(0.001)	0.0254(0.010)	0.0254(0.001)
Penetration Depth, MM (in)	0.762(0.030)	0.762(0.090)	0.762(0.030)	0.762(0.030)	-	-	0.762(0.030)	0.762(0.030)	0.762(0.030)
Max. Seal Wear Depth, MM (in)	None	0.0508(0.002)	-	-	-	-	0.508(0.020)	None	0.635(0.025)
Transfer to Seal	Heavy	Light	-	-	-	-	Light	Heavy	Moderate
Actual Surf. Temp., °K (°F)	1577(2380)	1539(2310)	1550(2330)	1608(2435)	-	-	1606(2430)	1561(2350)	1580(2385)
Max. Surf. Temp., °K (°F)	1872(2910)	1711(2620)	1989(3120)	2000(3140)	-	-	1650(2510)	1922(3000)	>1644(>2500)
Normal Load, K, (lb)	4.76(10.5)	11.79(26)	5.44(12)	1.63(8)	-	-	1.814(4)	4.989(11)	1.814(4)
Avg. Blade Wear, MM (in)	0.909(0.0358)	0.50(0.0197)	0.061(0.0024)	0.422(0.0166)	-	-	0.061(0.0024)	0.980(0.0386)	0.076(0.003)
Blade Pickup	Slight	Slight	Slight	Slight	-	-	Slight	Slight	Slight
VWR	Indeterminate	64.69	-	-	-	-	0.166	Indeterminate	0.09#
Remarks	Axial Cracks in Transfer	Axial Cracks in Transfer	70% of Zr O2 Layer Spalled During Rub Interaction	70% of Zr O2 Layer Spalled During Rub Interaction	60% of Zr O2 Layer Spalled During Heatup	50% of Zr O2 Layer Spalled During Heatup	Zr O2 Layer Partially Spalled During Heatup and Rub, mostly Outside Rub Path	Axial Cracks In Transfer	Axial and Circumferential Cracks

14

DIRECTION OF RUB
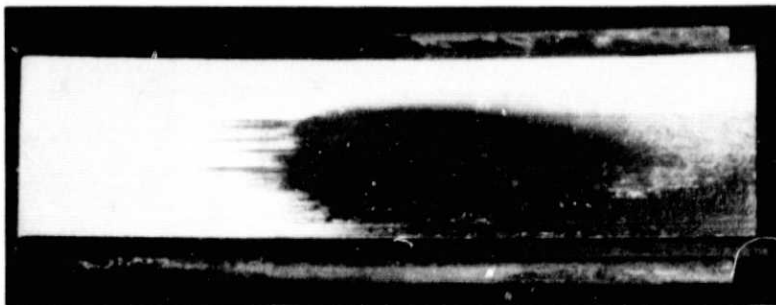
TEST SPECIMEN NO. 4
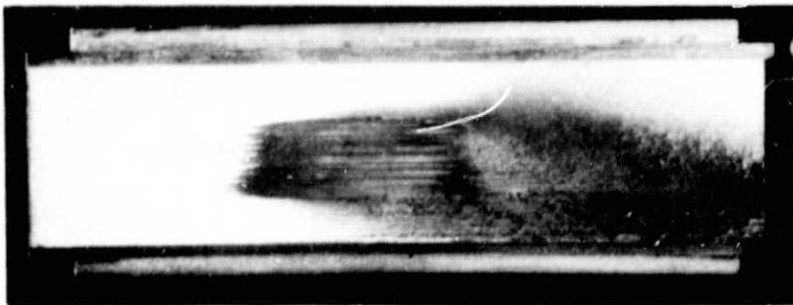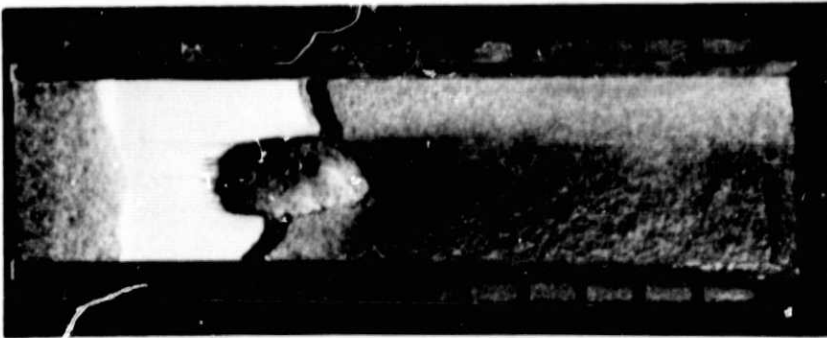
TEST SPECIMEN NO. 3

TEST SPECIMEN NO. 2

TEST SPECIMEN NO. 1
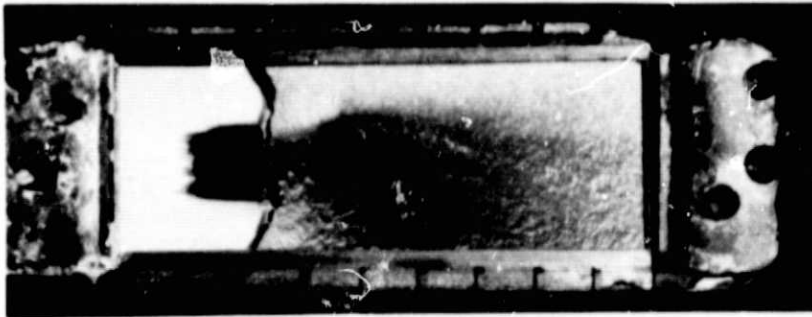
DIRECTION OF RUB

Figure 8   Results of Abradability Tests

3.3.2.2 Erosion Test Results

Erosion resistance of one specimen of each of the plasma sprayed ZrO_2/CoCrAlY seal systems, i.e., baseline and improved geometry, was evaluated by hot particulate rig testing at a ZrO_2 surface temperature of 1589°K (2400°F) and an impingement angle of 0.262 rad (15°).

Erosion tests were performed in the hot particulate erosion rig shown in Figure 9. The specimens were positioned at a distance of 3.81 cm (1.5 in) and 0.262 rad (15°) relative to the end of the combustor exit nozzle by a compound vise. The specimen was heated by impinging JP-5 fuel and air combustion products on the ZrO_2 surface of the specimen through a 1.905 cm (0.75 in) diameter exit nozzle. Specimen temperature and exit gas velocity were controlled by varying fuel and air flows.
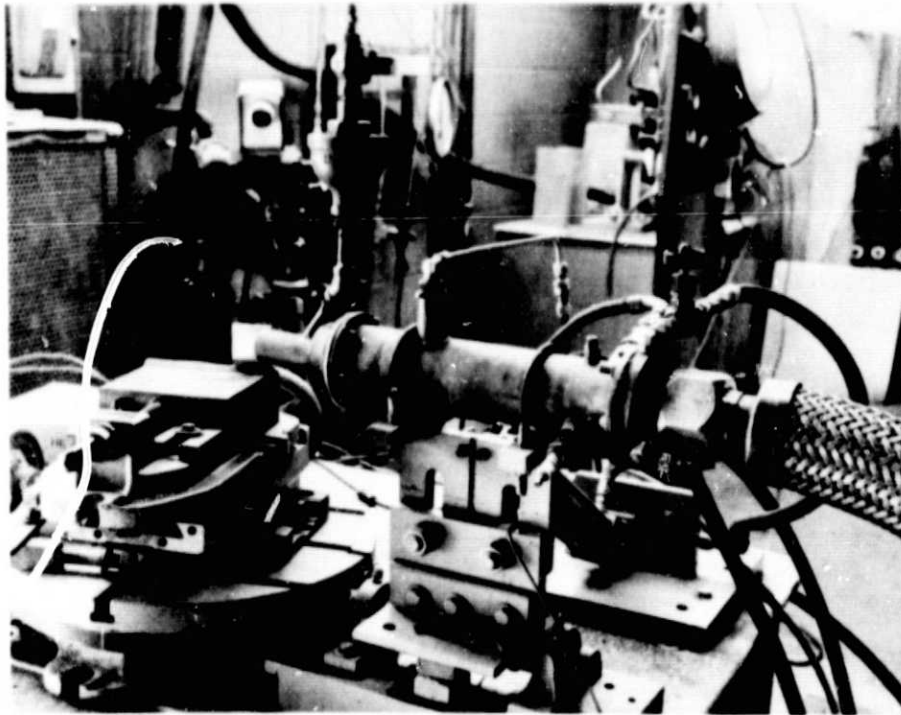
Figure 9   Hot Particulate Erosion Rig

After the specimen temperature and gas velocity were stabilized, particulate flow was initiated. The 80 grit Al_2O_3 particulate was gravity fed into a tube connected into the combustor exit nozzle approximately 5.08 cm (2 in) upstream of the nozzle end when it was picked up and accelerated to the specimen surface by the hot gas stream. Particulate flow rate was controlled by a precalibrated orifice in the storage

16

hopper discharge line. The weight of particulate used and the duration of particulate flow during the test was monitored to check the particulate flow rate.

Specimen temperature was measured optically on the ZrO_2 surface. Erosion wear was determined by measuring the weight loss of the specimen at five minute intervals.

The erosion specimen consisted of the composite seal system sprayed on a flat Hastelloy-X plate nominally 3.81 by 6.35 cm (1.5 by 2.5 in). A cap screw was welded to the center of the flat Hastelloy-X plate for mounting in the test fixture.

Erosion test results of both systems were similar as would be expected since both structures were sprayed in the same manner. The baseline erosion rate in Table 4 indicates a factor of 5 difference compared to the improved system. This difference is attributable to the corresponding factor of 5 in the particulate flow rates of the two tests.

A comparison of these test results and those of previous tests is also provided in Table 4. This comparison indicates the repeatability of the erosion resistance of the sprayed ceramic system. Figure 10 shows the baseline and improved geometry system specimens after testing.

Table No. 4

Erosion Test Data Summary

Case	Gas Velocity	Nozzle To Specimen Dist Cm. (in)	Surface Temp. ~$^\circ$K $^\circ$F	Impingement Angle~Rad	Particulate Type	Particulate Size	Particulate Flow Rate Kg/hr (lb/hr)	Erosion Rate gm/min(lb/min)	Remarks
NAS3-20623 Test No. 1	.35 Mach	3.81 (1.5)	1589 (2400)	.262	Al_2O_3	80 Grit	0.544 (1.199)	.004 (8.818)	922°K (1200°F system as-sprayed
NAS3-20623 Test No. 2	.35 Mach	3.81 (1.5)	1589 (2400)	.262	Al_2O_3	80 Grit	0.544 (1.199)	Undetermined	Baseline system as-sprayed
NAS3-19759 Test No. 5	.35 Mach	3.81 (1.5)	1589 (2400)	.262	Al_2O_3	80 Grit	2.72 (5.997)	0.0165(36.376)	Baseline system ZrO_2 delamination after 10 min.
NAS3-21390 Test No. 1	.35 Mach	3.81 (1.5)	1589 (2400)	.262	Al_2O_3	80 Grit	2.72 (5.997)	0.0108(23.810)	Baseline system machined
NAS3-21390 Test No. 2	.35 Mach	3.81 (1.5)	1589 (2400)	.262	Al_2O_3	80 Grit	0.544 (1.199)	0.0025(5.512)	Improved system machined
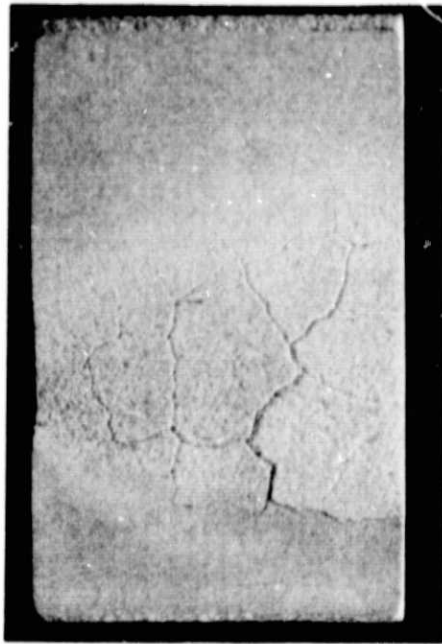
390 · 4 · 10

390 · 5 · 9

BASELINE SPECIMEN
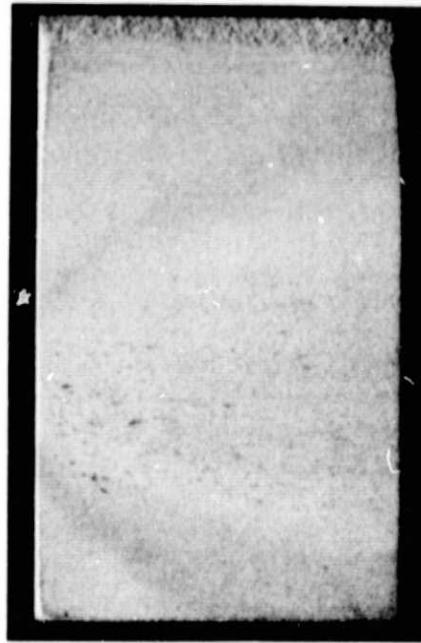
IMPROVED GEOMETRY SYSTEM

Figure 10   Tested Erosion Specimens

3.3.1.3 Thermal Shock Test Results

The durability of the sprayed ZrO_2/CoCrAlY seal system in an engine application will depend greatly on its capability to successfully survive the initial and subsequent thermal cycles corresponding to the engine operational conditions. This is the most difficult parameter to satisfy with a ceramic seal because of the relatively low strength (especially tensile strength) of ceramic materials and the large mismatch in thermal growth between ceramic and metallic materials. The graded, layered system was designed specifically to compensate for the layer difference in thermal expansion between the metal substrate and ceramic.

Cyclic thermal shock characteristics were evaluated by rig tests which subjected the seal specimens to a thermal cycle simulating the gas turbine engine cycle from idle to SLTO and back to idle, shown in Figure 11. A typical rig test cycle is also shown in Figure 11 and illustrates the close simulation produced by this rig.

Earlier thermal shock test results reported in NASA CR-135183 indicated thermal stress cracking initiated very early during the test. Analysis indicated cracking could occur in the first thermal cycle during acceleration to SLTO. Therefore, an attempt was made to better define when and where cracking was initiating by subjecting the seal specimens to an initial acceleration heatup cycle shown in Figure 12.
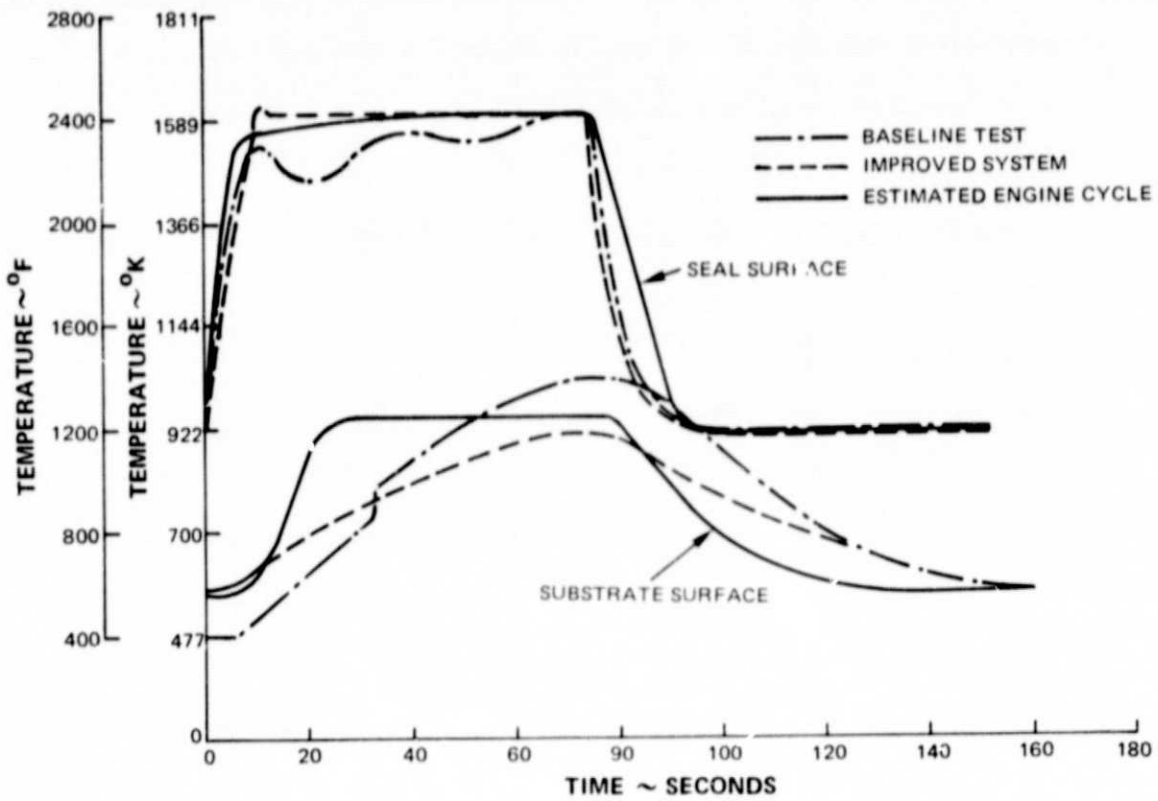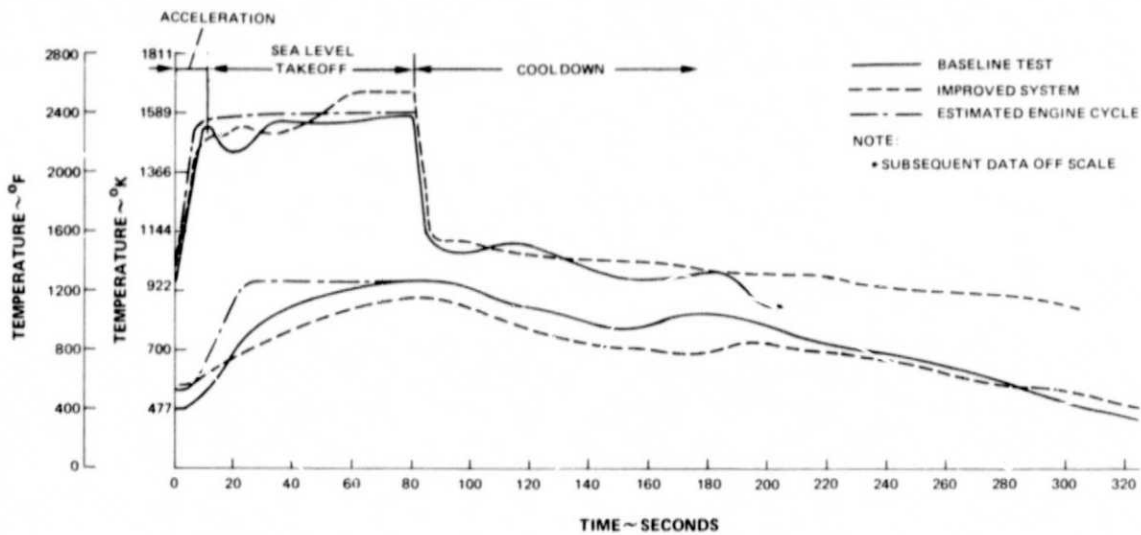
18

Figure 11   Thermal Test Cycle

Figure 12   Initial Acceleration Transient

19

The specimen was mounted in the cyclic thermal shock test rig, shown in Figure 2, by a fire brick holding fixture held by a water cooled copper fixture. A combination of oxygen-propane torches and cooling air jets was used to achieve the desired thermal cycles on the ZrO_2 and metal substrate surfaces. The torches were mechanically moved toward or away from the specimen at controlled rates to provide the required thermal cycle. Fixed cooling air jets were turned on or off or the flow was changed at predetermined intervals to meet the cycle requirements. The ZrO_2 and metal substrate surface temperatures were monitored continuously with an optical pryometer and thermocouples, respectively, and recorded on a strip chart.

Two specimens, one baseline and one improved geometry system, were tested. Both specimen were machined on the edges and ZrO_2 surface.

The baseline specimen exhibited tight laminar cracks at the 85/15 ZrO_2/CoCrAlY - 40/60 ZrO_2/CoCrAlY interface at three of the four corners (see Figure 13) as a result of exposure to the initial acceleration transient. No radial cracks were detected during this inspection. The first full simulated engine cycle resulted in additional laminar cracks at the ZrO_2 - 85/15 ZrO_2/CoCrAlY interface as well as radial cracks and the spalling of approximately a 1.27 cm (.5 in) long piece of ZrO_2 (see Figure 14).

The improved geometry specimen exhibited tight laminar cracks at the 85/15 ZrO_2/CoCrAlY - 40/60 ZrO_2/CoCrAlY interface at several locations (see Figure 15) as a result of exposure to the initial acceleration transient. No radial cracks were detected during this inspection. After the first full simulated engine cycle the laminar cracking propagated slightly and radial cracks were observed (see Figure 16). Inspection after twenty-five cycles revealed extensive laminar cracking at the 85/15 ZrO_2/CoCrAlY - 40/60 ZrO_2/CoCrAlY interface (see Figure 17). As a result of the 59th cycle approximately a 1.27 cm (.5 in) long section of ZrO_2 - 85/15 ZrO_2/CoCrAlY material spalled off causing the test to be terminated (see Figure 18).

The improved geometry system specimen was slightly modified (shortened) in an attempt to remove some laminar cracks which developed during machining. Approximately a 0.635 cm (.25 in) long end section of the specimen was removed. The success of this reoperation was questionable, however, because the machined surface was not smooth and some evidence of pitting was noticeable near the 85/15 ZrO_2/CoCrAlY - 40/60 ZrO_2/CoCrAlY interface. This condition may have been significant with respect to the initiation and extent of cracking.

20

2.54 MM
(0.10 IN.)

MAR-M-509
40/60 Z/M
85/15 Z/M
Z_RO_2

3.048 MM
(0.12 IN.)

1.524 MM
(0.06 IN.)

Z_RO_2
85/15 Z/M
40/60 Z/M
MAR-M-509

0.762 MM
(0.03 IN.)

3.048 MM
(0.12 IN.)

1.524 MM
(0.06 IN.)
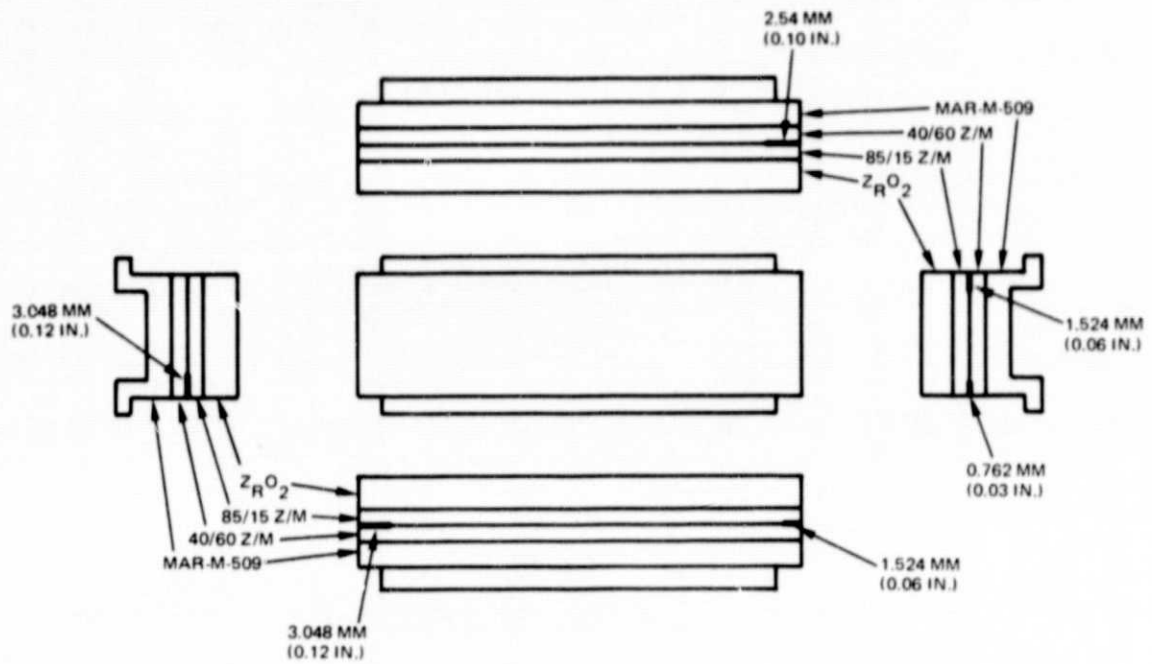
Figure 13   Baseline Specimen Initial Acceleration Transient Crack Map

Figure 14   Baseline Specimen First Engine Cycle Crack Map
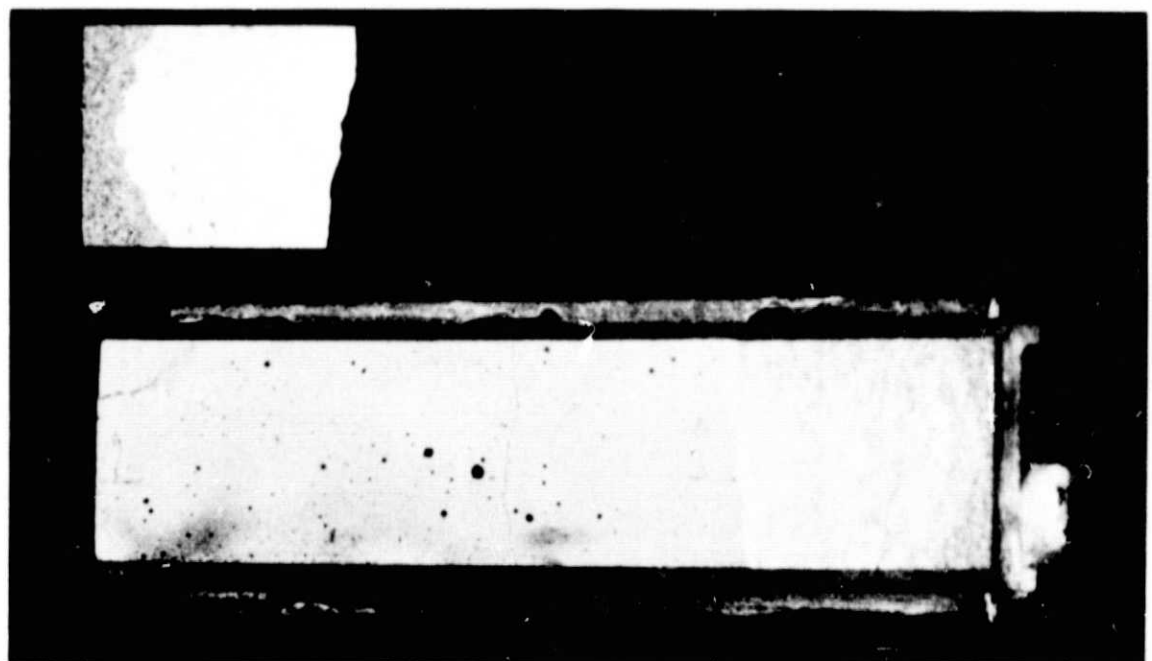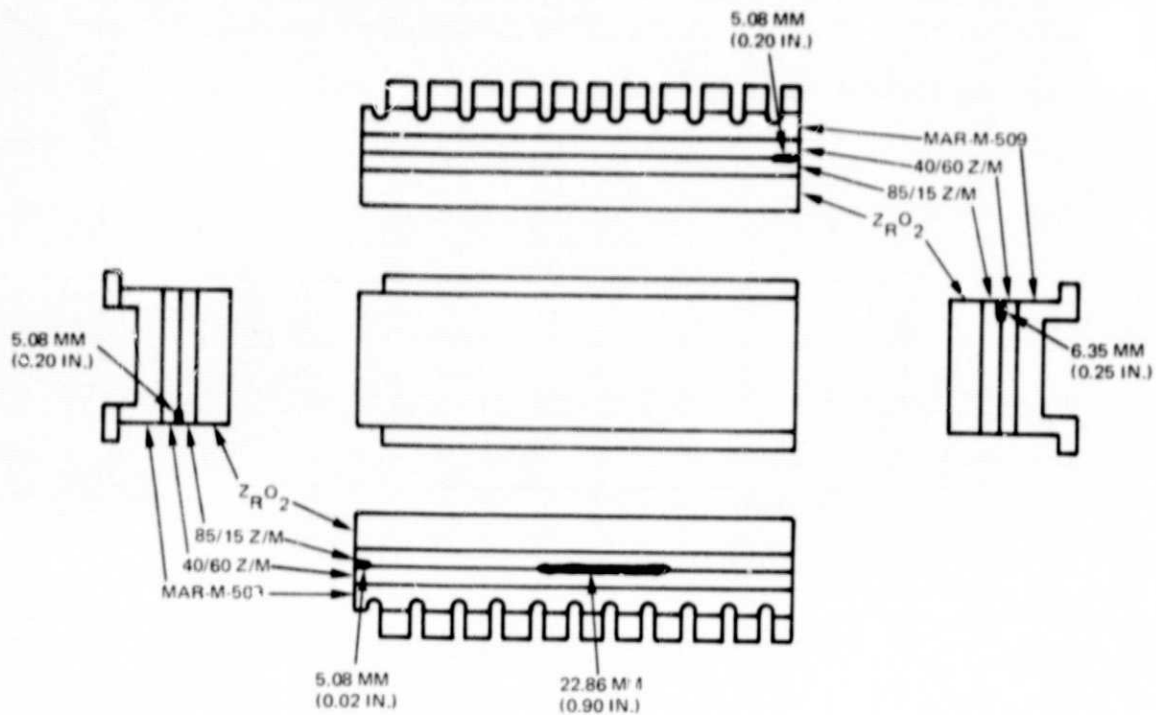
Figure 15   Improved Geometry System Specimen Initial Acceleration
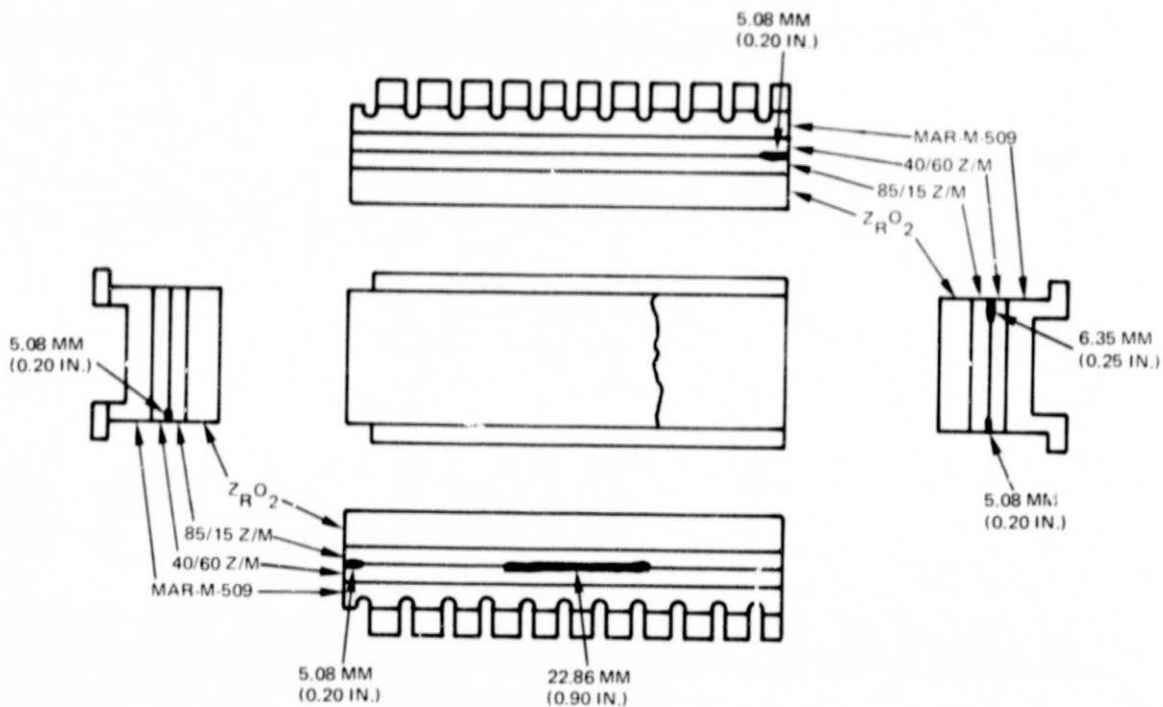   Transient Crack Map

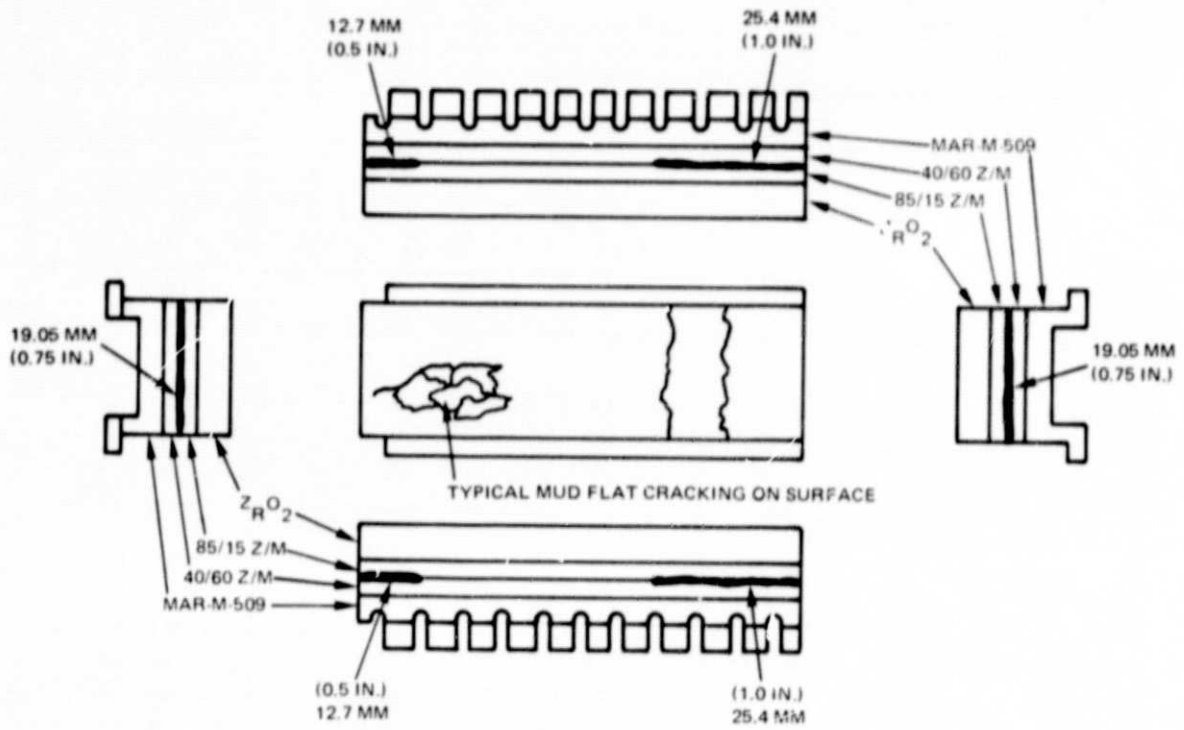Figure 16   Improved Geometry System 1st Engine Cycle Crack Map

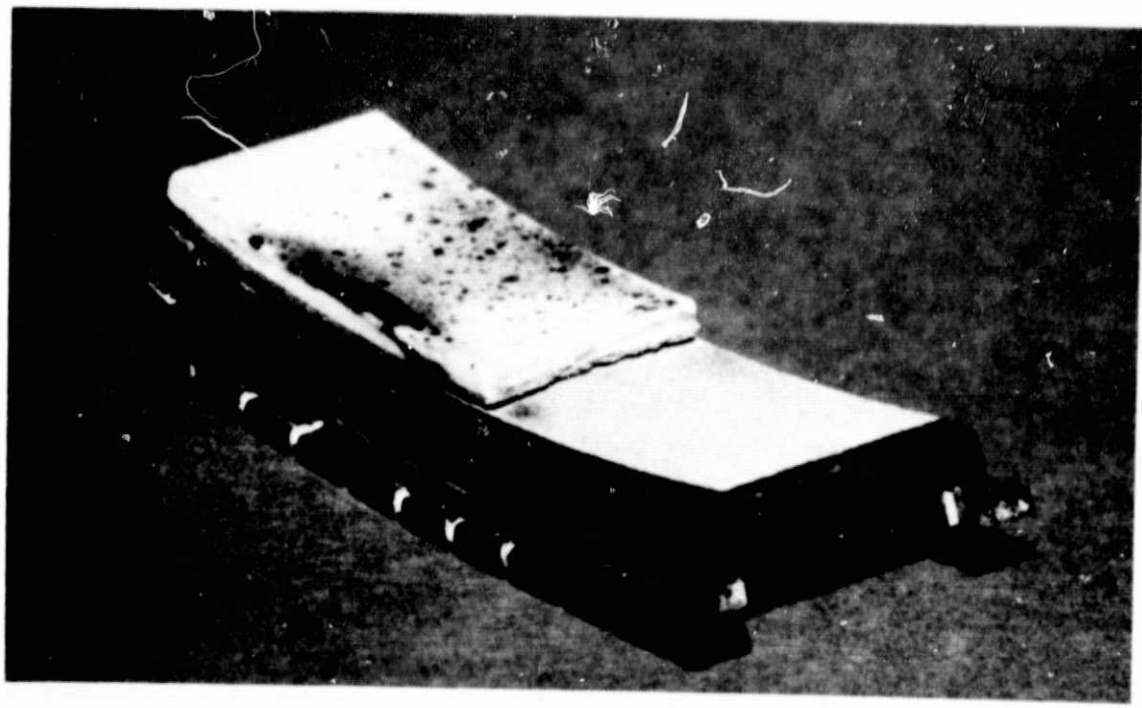Figure 17   Improved Geometry Specimen 25th Engine Cycle Crack Map

Figure 18   Improved Geometry System Specimen 59th Engine Cycle Crack
             Map

3.3.3 Analyses

3.3.3.1 Material Properties

Modulii of elasticity and rupture, thermal expansivity, thermal conduc-
tivity and tensile strength in the radial direction were determined for
each of the plasma sprayed ceramic and ceramic-metal layers for the
seal system. Specimens were machined from parts sprayed on mild steel
substrates. The substrates were removed from the specimens by machining.

Modulii of Elasticity and Rupture

Modulii of elasticity and rupture were determined at room temperature,
the maximum operating temperature for each layer, and at one interme-
diate temperature for each of the sprayed ZrO_2/CoCrAlY layers and the
ZrO_2 layer using the four-point flexure method. A strain gage, placed
at midspan and center of each specimen, was used to measure specimen
deflection for room temperature tests. Measurement of cross-head de-
flection was used to determined specimen deflection at temperatures
above strain gage capability 589^oK (600^oF). Test specimens measured
3.048 x 953 x .254 cm (1.20 x .375 x .100 in) and were prepared such
that the length of the specimen was in the circumferential direction.
Property characteristics were determined at 294, 1255, 1644^oK (70,
1800, 2500^oF) for the ZrO_2 layer, 294, 672, 1200^oK (70, 750,
1700^oF) for the 85/15 ZrO_2/CoCrAlY and 294, 589, 1033^oK (70, 600,
1400^oF) for the 40/60 ZrO_2/CoCrAlY.

Modulus of rupture and elasticity are presented in Table 5. The modulii
of rupture and elasticity increased with increasing percentage of
metallic supporting the trend observed in previous measurements. The
data was averaged with measurements taken under previous contracts and
these averaged results which include the data presented in Table 5 are
summarized in Figures 19 and 20. A least squares approach was used in
the data to define the relationship between the property and tempera-
ture. The measurements taken at the intermediate temperature point for
each of the materials resulted in a significant nonlinear relationship
for the modulus of elasticity for both the 85/15 ZrO_2/CoCrAlY and
40/60 ZrO_2/CoCrAlY layers. The curves for these values shown in
Figure 20 represent a significant change from the linear relationship
assumed in the past based on data of only the maximum and minimum
temperature points.

A review of the data plotted in Figures 19 and 20 shows that:

1. The modulus of rupture of the ZrO_2 is essentially constant at
    2.7 x 10^3 N/cm (4.0 ksi) to 1400^oK and decreases thereafter.

2. The rupture modulus for the 85/15 ZrO_2/CoCrAlY material is es-
    sentially constant at 4 x 10^3 N/cm^2 (5.8 ksi).

24

3. The rupture modulus for the 40/60 ZrO2/CoCrAlY material decreases with increasing temperature.

4. The modulus of elasticity of the ZrO2 material decreases with increasing temperature.

5. The modulus of elasticity of the 85/15 ZrO2/CoCrAlY and 40/60 ZrO2/CoCrAlY materials decreases with increasing temperature until approximately 700°K after which the modulus increases.

Table 5

Four Point Bend Test Data

	Temperature °K (°F)		Modulus of Rupture N/Cm² (KSI)		Modulus of Elasticity N/Cm²x10⁶ (10⁶ psi)	
Y2O3 Stabilized ZrO2	RT		2709.74	(3.93)	2.79	(4.05)
	RT		3399.24	(4.93)	2.84	(4.12)
	1255	(1800)	2178.82	(3.16)	0.69	(1.00)
	1255	(1800)	2040.92	(2.96)	1.21	(1.76)
	1644	(2500)	1337.63	(1.94)	0.83	(1.21)
	1644	(2500)	882.56	(1.28)	1.83	(2.65
85/15 ZrO2/CoCrAlY	RT		3592.30	(5.21)	2.14	(3.11)
	RT		3833.62	(5.56)	3.14	(4.55
	RT		3260.23	(4.74)	1.29	(1.87)
	RT		4130.11	(5.99)	1.85	(2.68)
	RT		4116.73	(5.97)	3.14	(4.55)
	672	(750)	4178.37	(6.06)	1.23	(1.78)
	672	(750)	3626.77	(5.26)	1.03	(1.49)
	672	(750)	3847.41	(5.58)	1.10	(1.59)
	672	(750)	3675.04	(5.33)	1.35	(1.96)
	1200	(1700)	~033.58	(5.85)	2.34	(3.39)
	1200	(1700)	3206.18	(4.65)	1.59	(2.30)
	1200	(1700)	3481.98	(5.05)	1.85	(2.68)
	1200	(1700)	3247.55	(4.71)	2.59	(3.75
40/60 ZrO2/CoCrAlY	RT		14479.50	(21.0)	10.62	(15.4)
	RT		16410.10	(23.8)	5.65	(8.20)
	RT		15237.95	(22.1)	4.58	(6.64)
	589	(600)	16410.10	(23.8)	3.42	(4.96)
	589	(600)	17306.45	(25.1)	3.10	(4.49)
	589	(600)	17168.55	(24.9)	3.55	(5.15)
	1033	(1400)	16548.00	(24.0)	3.83	(5.55)
	1033	(1400)	15789.55	(22.9)	3.56	(5.17)
	1033	(1400)	16203.25	(23.5)	2.81	(4.08)
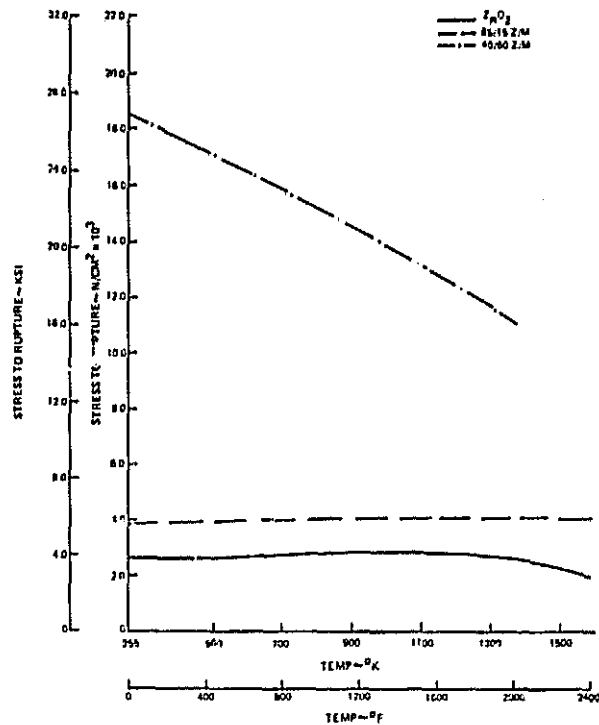
Figure 19   Average Modulus of Rupture
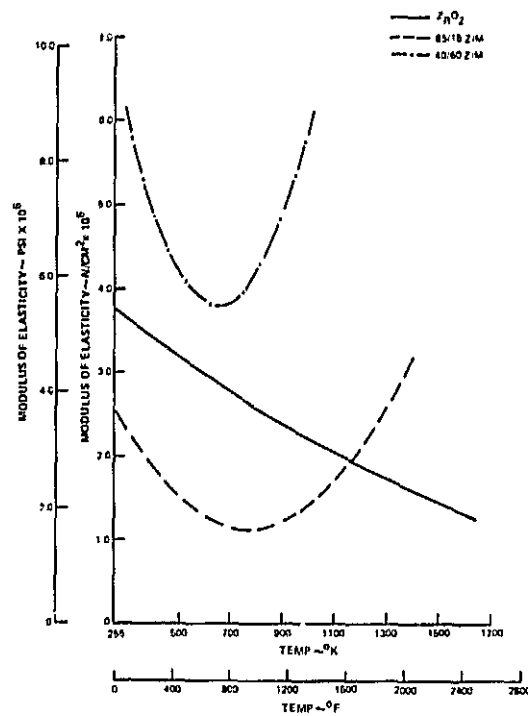
Figure 20   Average Modulus of Elasticity

26

Thermal Expansion

The thermal expansivity for each material layer in the plasma sprayed ZrO_2/CoCrAlY seal system was measured in the circumferential direction. Specimens measured 2.540 x 0.508 x 0.254 cm (1.0 x 0.2 x 0.1 in).

After being accurately measured in the 2.540 cm (1.0 in) direction, the specimens were instrumented with a Netzch Electronic Automatic Recording Dilatometer. The system was placed in the center zone of a closed chamber which was evacuated and then backfilled with helium. The specimens were then programmed for temperature rise and equilibrium at approximately 100°K (180°F) intervals from 293°K (68°F) to 1202°K (1704°F), 1341°K (1954°F) and 1608°K (2434°F) for 40/60 ZrO_2/CoCrAlY, 85/15 ZrO_2/CoCrA.Y and ZrO_2 materials, respectively. An equivalent program for temperature fall and equilibrium was also implemented. The rate of temperature rise and fall was approximately 5°K/min (9°F/min).

The ZrO_2 material demonstrated a very definite shrinkage above 1473°K (2192°F) during the first thermal cycle, as shown in Figure 21. Total shrinkage of 0.36 percent was measured. Subsequent cycles did not exhibit this shrinkage and were very repeatable. Figure 22 shows data typical of these subsequent cycles.

The 40/60 and 85/15 ZrO_2/CoCrAlY materials demonstrated fairly repeatable thermal growths both during heating and cooling and from cycle to cycle although some tendency to grow was seen. Data for these layers is shown in Figures 23 and 24, respectively.
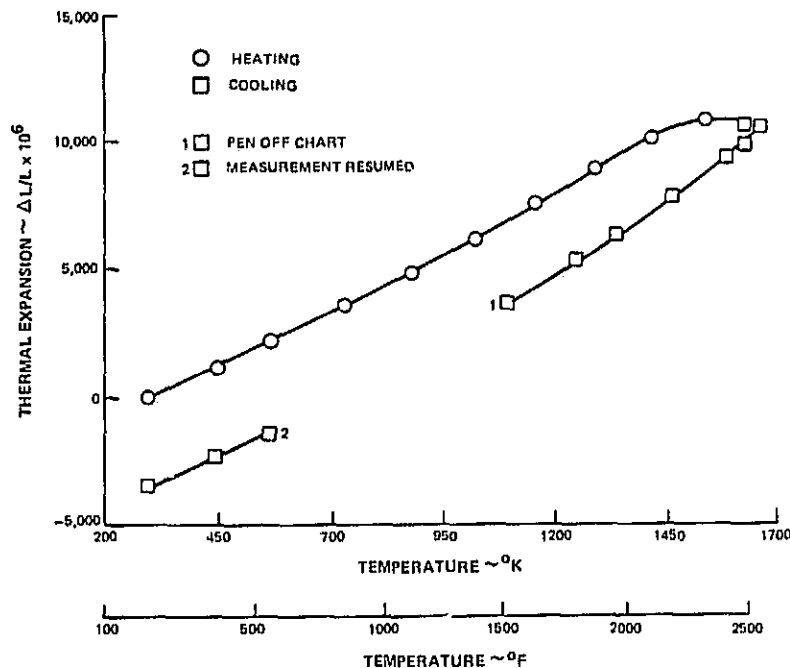
Figure 21   Thermal Expansion Plasma Sprayed ZrO_2 First Cycle

27
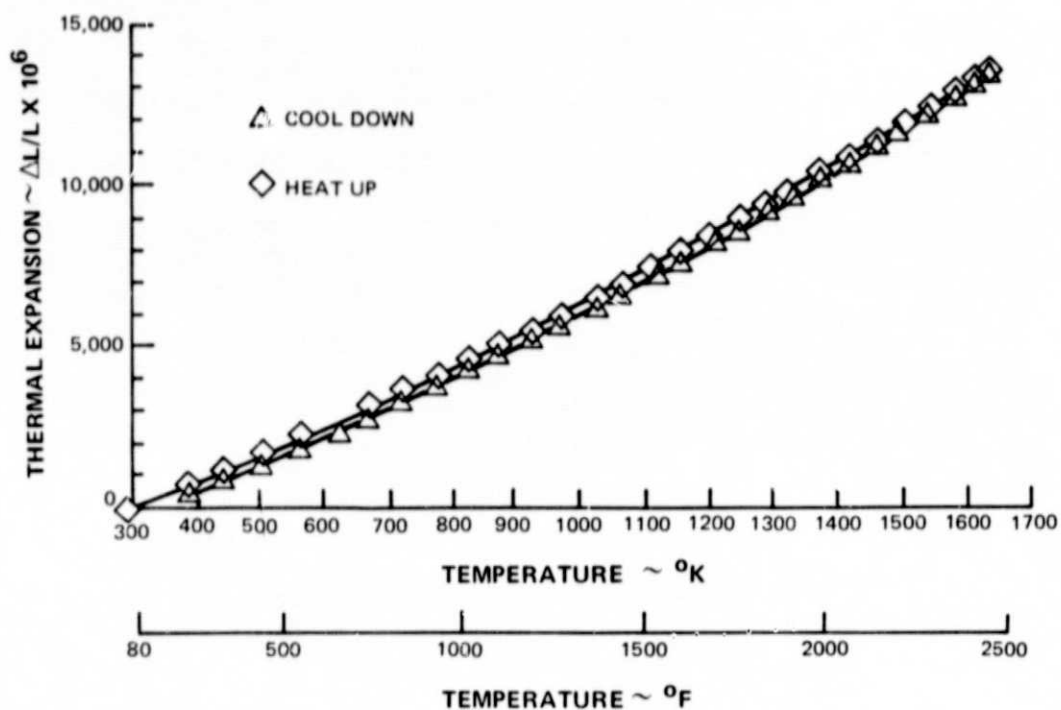
Figure 22   Thermal Expansion Plasma Sprayed ZrO_2 Third Cycle
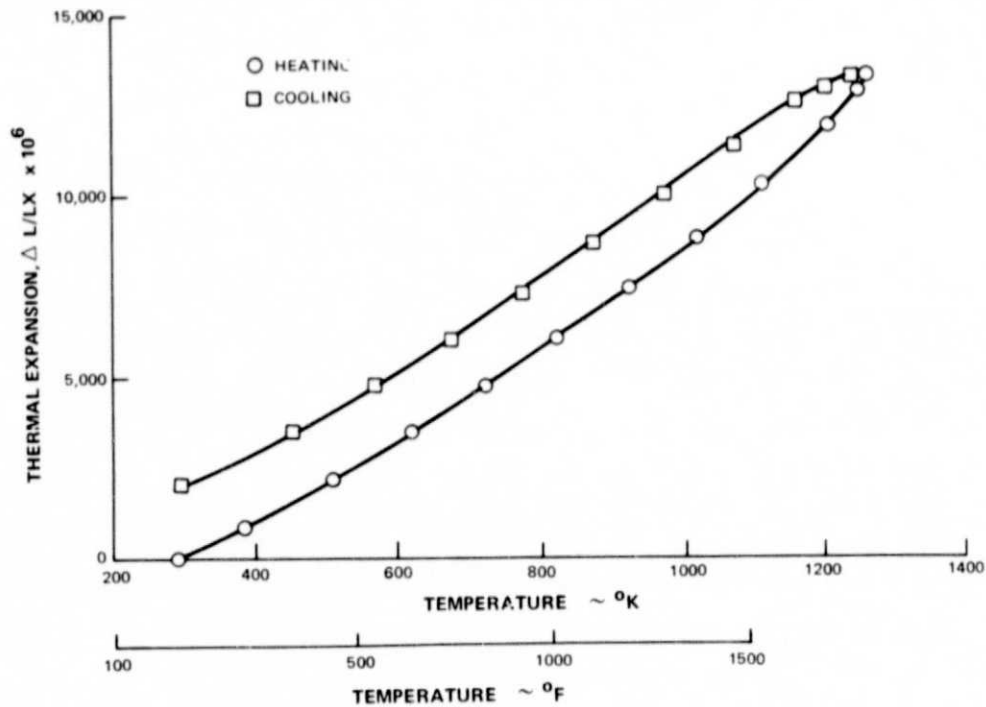
Figure 23   Thermal Expansion of Plasma Sprayed 85/15 $ZrO_2/CoCrAlY$

28
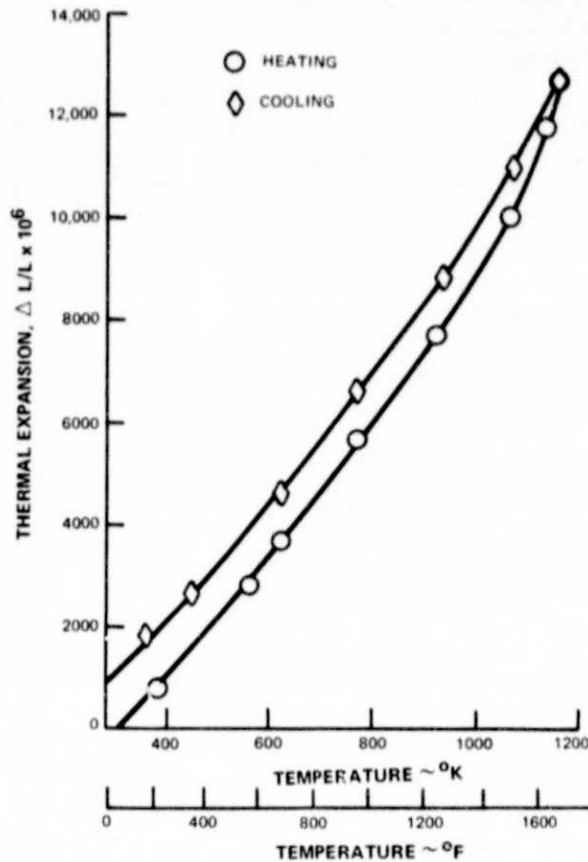
Figure 24   Thermal Expansion Plasma Sprayed 40/60 ZrO_2/CoCrAlY

Thermal Conductivity

Thermal conductivity was determined for each material layer in the plasma sprayed ZrO_2/CoCrAlY seal.

Thermal conductivity (K) was determined by measuring the thermal diffusivity (α), density (d), and specific heat (Cp) and taking the product of these three measurements (K = α Cpd).

Thermal diffusivity was measured by the highly developed laser flash technique. In this technique, a flash of radiant energy is deposited uniformly over one surface of a homogeneous specimen during a negligible time duration and the heat pulse diffuses unidirectionally to the opposite face. The diffusivity was calculated from the specimen thickness and the time required for the rear face temperature rise to reach a known percentage of its maximum value. The specimen used was shaped in the form of a disk, with a diameter of 1.7907 cm (.705 in) and a thickness of .1270 cm (.05 in). The accuracy in measuring the thermal diffusivity is considered to be $\pm2\%$.

Specific heat, measured on a .635 cm (.25 in) diameter disk .254 cm (.10 in) thick, was measured in Argon using a standard Perkin-Elmer Model DS C-2 differential scanning calorimeter. The specimen holder and a holder for reference, equipped with heaters and temperature sensors detected fluctuations of the specimen holder temperature with respect to the reference as both were heated. A high gain, closed-loop electronic system provided differential electrical power to the heaters to compensate for fluctuations. This differential power was read out directly in millicalories per second and is equivalent to the rate of energy absorption or evolution of the specimen. The specific heat was determined by comparing this rate with the rate measured during the heating of a known mass of sapphire. The accuracy of this device is $\pm 3\%$. The upper limit for this test equipment is $1000^{\circ}K$ ($1340^{\circ}F$). Above this temperature values were determined by extrapolation.

Density was determined by accurately measuring the apparent volume and mass of the specific heat specimen and then dividing the mass by the volume.

The resultant thermal conductivity values for all three material layers are presented in Table 6. These values are similar to previously measured values at room temperature, however, at elevated temperatures these values are lower than previously measured by approximately 40% for the ZrO_2, 50% for the 85/15 ZrO_2/CoCrAlY and 300% for the 40/60 ZrO_2/CoCrAlY layer. The technique utilized to measure thermal conductivity for this program is different and more accurate than that utilized previously. Each layer of the system was tested under this program whereas previous measurements were taken of the ZrO_2 layer and the composite and values of the intermediate layers were then estimated based on the percentage of ZrO_2 in each layer. Because of the improved technique utilized under this program the values measured and reported in Table 6 are considered to be more accurate than previous values.

Table No. 6

Thermal Conductivity of Sprayed Ceramic Seal Constituents
$W/m^{\circ}K$ ($BTu\ in/HrFt^2\ {}^{\circ}F$)

Temperatures $^{\circ}K$ ($^{\circ}F$)		ZrO_2		85/15 Z/M		40/60 Z/M	
RT		0.47	(3.29)	0.55	(3.83)	1.08	(7.50)
373	(212)	0.46	(3.19)	0.54	(3.75)	1.11	(7.73)
473	(392)	0.46	(3.18)	0.53	(3.68)	1.20	(8.32)
573	(572)	0.45	(3.15)	0.53	(3.67)	1.31	(9.10)
673	(752)	0.45	(3.13)	0.54	3.72)	1.41	(9.79)
773	(932)	0.45	(3.11)	0.54	(3.77)	1.49	(10.33)
873	(1112)	0.44	(3.08)	0.55	(3.84)	1.54	(10.69)
973	(1292)	0.45	(3.11)	0.56	(3.88)	1.64	(11.40)
1073	(1472)	0.46	(3.16)	0.56	(3.91)	1.78	(12.33)
1148	(1607)					1.91	(13.24)
1173	(1652)	0.46	(3.17)	0.56	(3.92)		
1248	(1787)			0.57	(3.95)		
1273	(1787)	0.47	(3.27)				
1373	(1787)	0.47	(3.26)				
1473	(2192)	0.51	(3.52)				
1573	(2372)	0.53	(3.67)				
1648	(2507)	0.54	(3.77)				

Hardness

Superficial Rockwell 45Y hardness was measured on the as-sprayed ZrO_2 surface of three of the abradability specimens, two baseline and one improved geometry system. Measurements were taken on machined surfaces after testing.

The average hardness for all three specimens were similar and within the range of specimens (see Table 3) measured under previous programs.

Tensile Strength In The Radial Direction

Tensile strength in the radial direction was determined for each material layer in the plasma sprayed ZrO_2/CoCrAlY seal system.

The wafer shaped specimens (1.27 cm diameter and .254 cm thickness (.5 in diameter and .1 in thickness)) were machined from the substrates and bonded to modified stainless steel bond bars for testing.

Measurements were performed at room temperature and at the highest elevated temperature possible (422°k (300°F)). The maximum temperature for these measurements were limited by the temperature capability of current state of art bonding techniques. FM-100 adhesive (American Cyanamid) was used for room temperature tests and FM-150 adhesive was used for elevated temperature tests.

Figure 25 illustrates the separation in approximately the middle of the specimen which was typical of the results of measurements of each the ZrO_2 and 85/15 ZrO_2/CoCrAlY materials.

0.25 in.
1 cm.

Figure 25   Results of Radial Strength Measurement of ZrO_2 Illustrating Typical Fracture

Results of the radial strength measurements are listed in Table 7. The tensile strength of both the ZrO_2 and 85/15 ZrO_2/CoCrAlY in the radial direction at room temperature was appreciably less, approximately 1/5 the strength of the materials in the circumferential direction as measured by four point bend technique. Additional data should be generated and analyzed, however, to more accurately define the strength temperature relationship in the radial direction. The tensile strength testing of the 40/60 ZrO_2/CoCrAlY in the radial direction was inconclusive because of machining difficulties encountered in specimen preparation which resulted in partial delamination and contributed to the very low measured data.

Table No. 7

Radial Tensile Strength of Sprayed Ceramic Seal

Material	Temp. $^\circ K$ ($^\circ F$)	Tensile Strength Radial Direction N/Cm^2 (PSI)
ZrO_2	RT	508.85 (738)
ZrO_2	RT	521.26 (756)
ZrO_2	RT	587.45 (852)
ZrO_2	422 (300)	333.03 (483)
85/15 Z/M	RT	646.06 (937)
85/15 Z/M	RT	682.61 (990)
85/15 Z/M	RT	595.7ᵇ (864)
85/15 Z/M	422 (300)	353.02 (512)
40/60 Z/M	RT	104.11 (151*)
40/60 Z/M	RT	32.41 (47*)
40/60 Z/M	RT	304.76 (442)
40/60 Z/M	422 (300)	105.49 (153)

* Partial Delamination of Specimen

Residual Stresses

Two specimens, one of the baseline and one with improved geometry were used to determine residual stress distributions. Refined strain measuring techniques, developed through in-house development programs were utilized which improved the accuracy of the measurements in comparison to previous data.

Residual stress distribution in the specimen was calculated using an infinite flat plate composite material model to determine a Stress Free Temperature (SFT) distribution through the specimen which would match the measured strains at the gage location in the circumferential direction. The stress free temperature distribution is the temperature distribution necessary to produce a zero stress distribution throughout the part.

32

A comparison of these results to those previously determined (NAS3-19759 and NAS3-20623) is provided in Figure 26. Larger discontinuities in the SFT at the 85/15 ZrO2/CoCrAlY - 40/60 ZrO2/CoCrAlY and the 40/60 ZrO2/CoCrAlY - substrate interfaces were identified. This increase in SFT discontinuity causes an increase in resultant operating stresses. Crack initiation during thermal shock testing occurred at the 85/15 ZrO2/CoCrAlY - 40/60 ZrO2/CoCrAlY interface, the location of the larger discontinuity in the SFT.
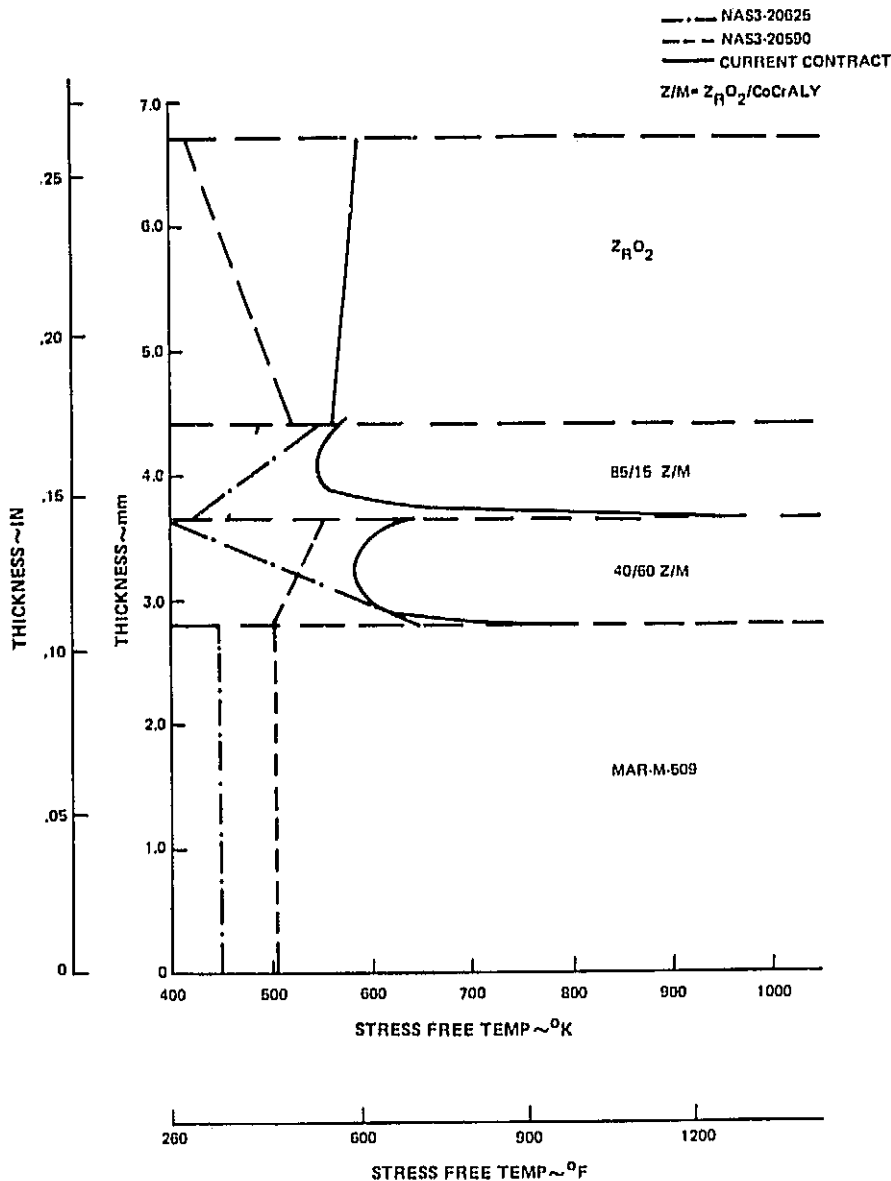

Figure 26   Stress Free Temperature Comparison Curve

The stress free temperature distribution calculated for the two systems were virtually identical verifying the previous assumption that substrate configuration for residual stress determination does not significantly affect the stress free temperature distribution.

3.3.3.2 Stress Analyses Correlation With Cyclic Thermal Shock Rig Test Results

Analyses of both the baseline and improved geometry systems for actual rig test thermal cycles were performed. SFT distribution based on measured residual strains in the ZrO_2/CoCrAlY seal system specimens and average physical properties were used in this analysis.

Temperature distributions were calculated based on measured temperatures on the ZrO_2 and metal substrate surfaces and thermal properties of the spray system materials using the two dimensional finite element computer program reported in NASA CR-135387. Temperatures were assumed uniform in the axial-circumferential plane thus only radial gradients were calculated. Figure 11 provides a comparison of the actual baseline and improved geometry test cycles to a typical estimated engine cycle. The ZrO_2 surface temperature for both tests matched the estimated engine cycle extremely well during all time points. The substrate surface acceleration temperature rate for both tests was not as rapid as the estimated engine cycle. This condition resulted in a large front to back surface temperature differential and correspondingly higher thermal stresses, thus resulting in a conservative acceleration portion of the thermal cycle.

The substrate surface deceleration temperature rate for both tests was not as rapid as the estimated engine cycle. This condition resulted in a lesser front to back surface temperature differential and correspondingly lower thermal stresses, thus resulting in a less severe deceleration simulation. However, since the deceleration condition is not limiting from a stress standpoint, the overall cyclic thermal shock tests were considered a slightly more severe simulation of predicted engine condition.

Calculated thermal distributions were used in a two dimensional finite element plane stress computer program to estimate stress distributions. The thermal distribution used to determine the stresses during SLTO conditions was that representative of steady state condition of 75 sec into the thermal cycle. The thermal distribution through the seal for the acceleration and deceleration transients were defined by an analyses of the distribution through the seal at a number of time intervals into the transients. Ceramic surface temperatures (top) and substrate (bottom) temperature were evaluated and the temperature distribution of 10 sec into acceleration and approximately 90 sec into deceleration which represented the largest and smallest differences between the top and bottom temperatures of the ceramic seal. The corresponding temperature distribution through the seal was used to estimate stresses in the seal during the transient operation conditions.

34

An analyses of the circumferential plane was used to define the internal stresses in the system since previous effort had determined that stresses in that plane were most severe.

Stress distributions during acceleration, SLTO and deceleration were evaluated. A summary table of the maximum stresses, which were at the interfaces, is provided in Table 8. The stresses were determined by scanning the finite element stress output for each of the geometry condition analyzed and identifying the maximum principle stress in each of the graded material layers.

Results of the analyses correlated very well with cyclic thermal shock rig test results. For the baseline test, crack initiation was predicted analytically at the 85/15 ZrO_2/CoCrAlY - 40/60 ZrO_2/CoCrAlY interface edge during the acceleration portion of the cycle (1.20 stress/strength ratio Table 8). Tight laminar cracking was observed in this area. After the acceleration abort test cycle, the analysis defined a stress/strength ratio of 1.78 and 1.90 at the ZrO_2 -85/15 ZrO_2 CoCrAlY interface close to the center of the specimen as a result of thermal environment at SLTO and deceleration to idle. Inspection of the baseline parts after exposure to SLTO and deceleration revealed that the ceramic layer had spalled at the ZrO_2 - 85/15 ZrO_2/CoCrAlY interface about 1.27 cm (.5 in) away from the center.

A similar correlation of analysis and test was shown for the improved system. Analysis predicted crack initiation at the 85/15 ZrO_2/CoCrAlY interface during acceleration with 1.01 stress/strength ratio and a laminar crack did result after the acceleration portion of the thermal shock test. Cracks in the location did propagate after one complete cycle (exposure to SLTO and deceleration). The stress/strength ratio at this location, 1.15, under those conditions was essentially the same as the value at the 40/60 - ZrO_2/CoCrAlY substrate interface but probably more effective because of the stress riser at the existing crack location.

Metallography

Both of the cyclic thermal shock specimens were microsectioned after testing to identify any structural changes due to thermal exposure and to indicate location of cracks. Typical microsections of the baseline and improved geometry specimens are shown in Figures 27 and 28 respectively.

A comparison of Figures 27 and 28 indicates the similarity of the structures and is an indication of the repeatability of the spray fabrication procedure.
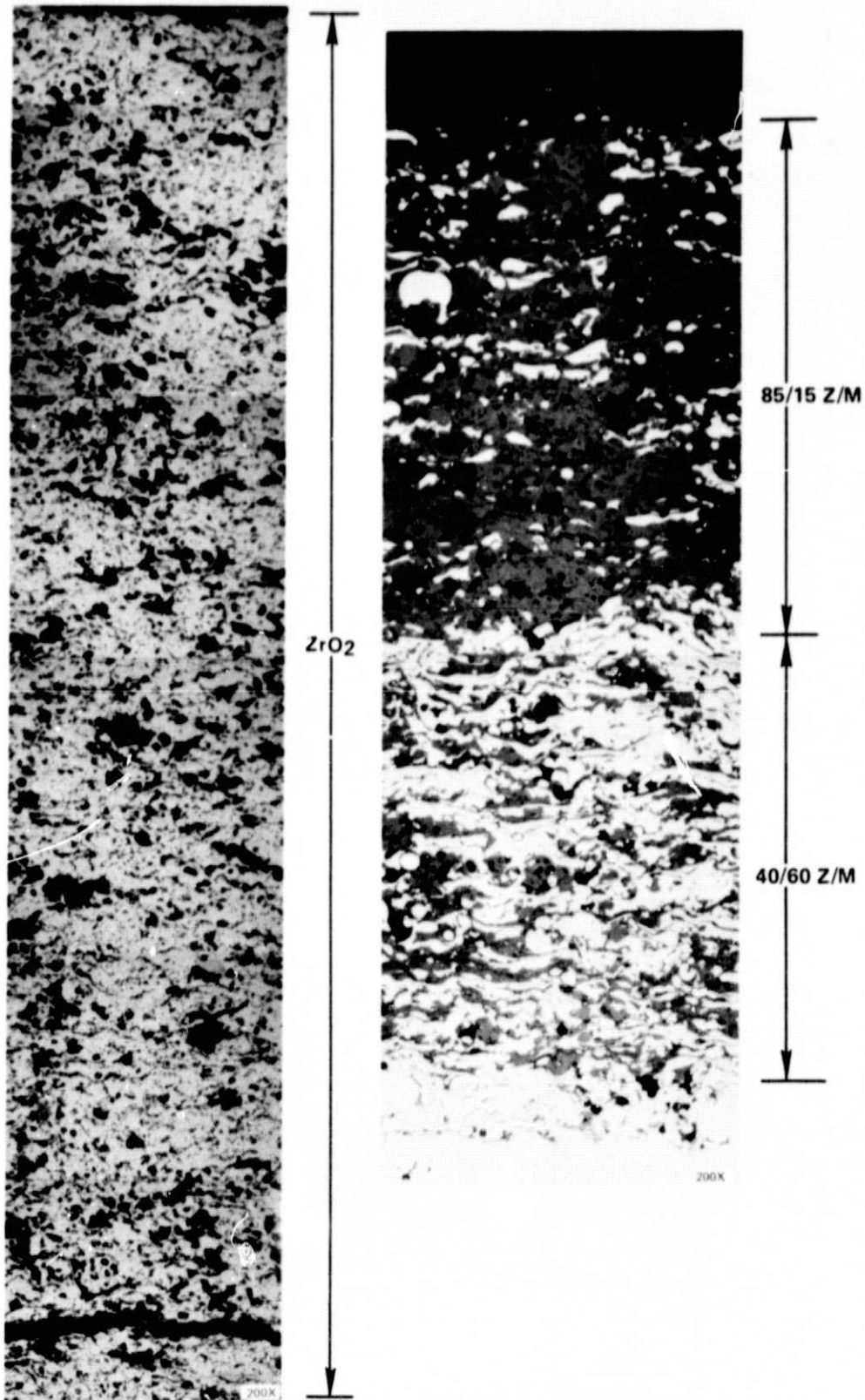
Table No. 8

Stress/Strength Summary Table

Accel

No.	System	Thermal Cycle	ZrO2 85/15 Interface	X Coord	85/15 40/60 Interface	X Coord	40/60 Sub Interface	X Coord	85/15 Sub Interface	X Coord
1	Baseline (1)	Est. Eng	1.00	1.3058	1.13	1.2708	.77	1.1565	----	----
2	Baseline (2)	Test	1.07	1.3058	1.20	1.2708	.78	1.1565	----	----
3	Improved (1)	Est. Eng	.71	1.3292	1.05	1.2358	.79	.5900	----	----
4	Improved (2) Geometry	Test	.75	1.3292	1.01	1.2592	.77	.5900	----	----
5	2 Layered (1) Geometry	Est. Eng	.59	1.3175	----	----	----	----	1.32	.59
6	.045 ZrO2 (1) Improved Geometry	Est. Eng	.49	1.3525	.94	1.1775	.70	.5700	----	----

SLTO

No.	System	Thermal Cycle	ZrO2 85/15 Interface	X Coord	85/15 40/60 Interface	X Coord	40/60 Sub Interface	X Coord	85/15 Sub Interface	X Coord
1	Baseline (1)	Est. Eng	1.74	.370	1.36	.370	1.30	.8415	----	----
2	Baseline (2)	Test	1.78	.370	1.60	.370	1.62	1.3992	----	----
3	Improved (1)	Est. Eng	.74	1.2825	1.17	1.1565	1.22	.6314	----	----
4	Improved (2) Geometry	Test	.70	1.3175	1.15	1.3292	1.16	.6315	----	----
5	2 Layered (1) Geometry	Est. Eng	.84	.9465	----	1.2195	----	----	1.49	1.2708
6	.045 ZrO2 (1) Improved Geometry	Est. Eng	.48	1.3525	.94	1.2195	.85	.6945	----	----

DECEL

No.	System	Thermal Cycle	ZrO2 85/15 Interface	X Coord	85/15 40/60 Interface	X Coord	40/60 Sub Interface	X Coord	85/15 Sub Interface	X Coord
1	Baseline (1)	Est. Eng	.57	.3300	.84	.3100	.67	.9255	----	----
2	Baseline (2)	Test	1.90	.3300	1.22	1.3292	1.50	1.3992	----	----
3	Improved (1)	Est. Eng	.30	1.3175	.82	1.1775	.65	.6105	----	----
4	Improved (2) Geometry	Test	.65	.8415	.79	1.2195	.86	1.3992	----	----
5	2 Layered (1) Geometry	Est. Eng	.27	.450	----	----	----	----	1.05	1.3292
6	.045 ZrO2 (1) Improved Geometry	Est. Eng	.18	1.3525	.68	1.1775	.54	1.0725	----	----

Note:

✓ indicates actual crack location

◯ indicates max stress/strength in system

(1) Estimated engine thermal cycle used to evaluate configuration changes to select a back-up system.

(2) Actual rig test thermal cycle used to correlate analyses to test results.

36

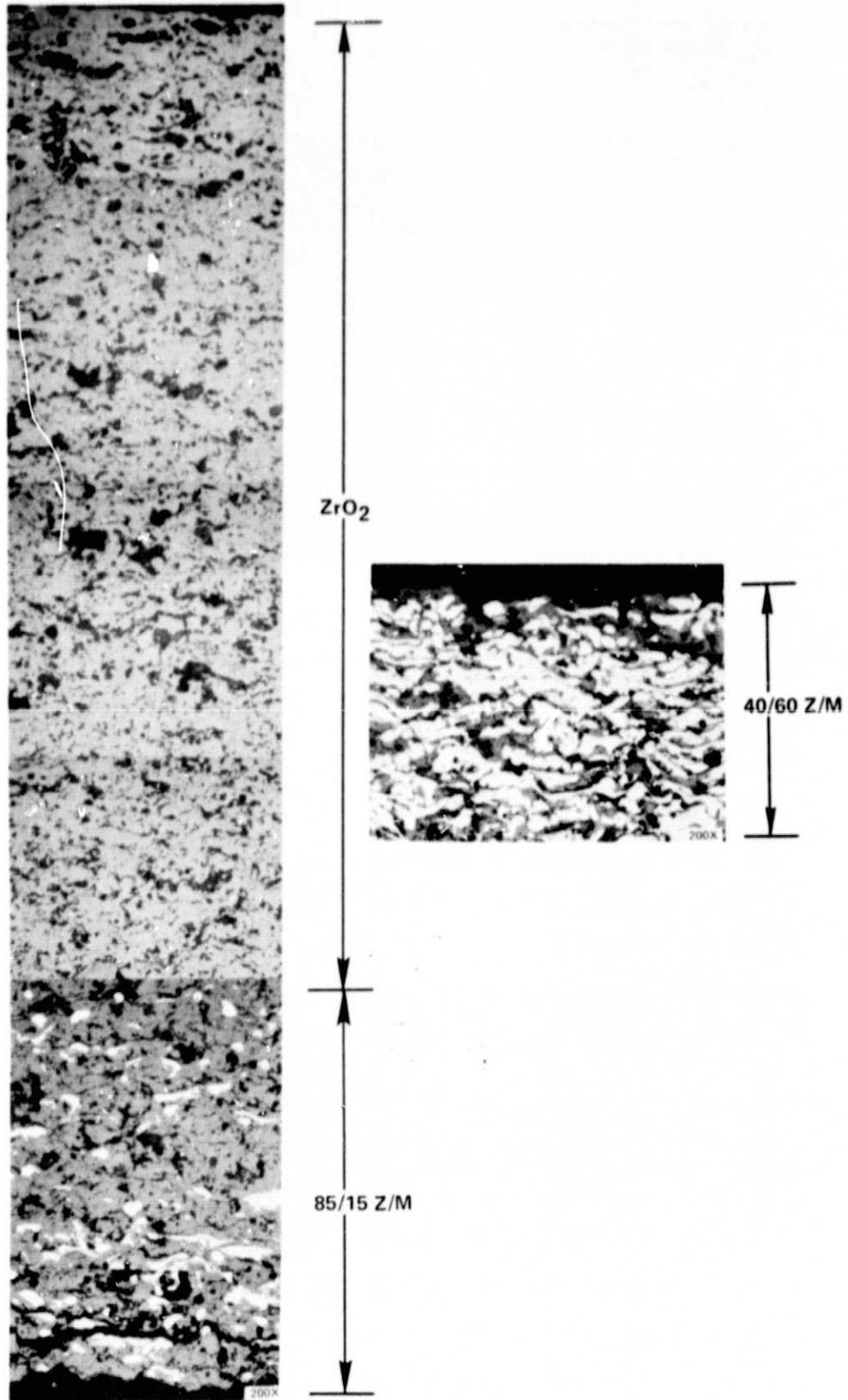Figure 27   Microstructure of Baseline System

Figure 28   Microstructure of Improved Geometry System

The crack location shown for the baseline system in Figure 27 is directly at the ZrO_2 - 85/15 ZrO_2/CoCrAlY interface and extends along the entire axial and a majority of the circumferential plane. This crack occurred during the SLTO condition. Not shown in the metallography is another crack at the 85/15 ZrO_2/CoCrAlY - 40/60 ZrO_2/CoCrAlY interface. This crack occurred during acceleration and extended approximately .254 cm (.1 in) both axially and circumferential at three of the four corners. The two cracks were joined by radial crack after the first full simulated engine cycle.

The crack in the improved geometry system initiated near the 85/15 ZrO_2/CoCrAlY - 40/60 ZrO_2/CoCrAlY interface. The crack extended along the full axial length either exactly at the interface or up to 1.27 cm into the 85/15 ZrO_2/CoCrAlY layer.

3.3.3.3 Backup System Analyses

Analysis was conducted to define a configuration which would result in lower stresses which could be fabricated as a "back-up" system. Two configurations were analyzed. The first, shown as No. 5 on Table 8 replaces the 40/60 ZrO_2/CoCrAlY material to eliminate the 85/15 - 40/60 ZrO_2/CoCrAlY interface. The stress/strength ratio was estimated at 1.32 at acceleration and 1.49 at SLTO and therefore this configuration was not judged to be acceptable. the second configuration, a 0.45 in ZrO_2 thickness reduced stresses by 20% and eliminated all stress/strength ratios greater than 1. This configuration was recommended to, and approved by, the NASA Project Manager and parts will be fabricated and delivered to NASA for testing.

4.0 CONCLUSIONS AND RECOMMENDATIONS

4.1 Conclusions

The close correlation between stress analysis and cyclic thermal shock results supports the accuracy of the design system. Analysis indicating that thermal stresses can be reduced to below the strength of the constituent material by reducing the zirconia layer thickness increases the confidence in attaining the objective of designing a sprayed graded ZrO_2/metallic/seal system for turbine application.

An investigation of the reduced cyclic thermal shock resistance of specimens tested under this contract in comparison to results reported in NASA CR-135387 led to identification of a possible cause. Several instances of crack initiation were observed during machining of specimens for rig testing which substantiated the need for improved fixturing and tighter controls. Results reported in NASA CR-135387 were for the as-sprayed, non-machined state. It is possible therefore that microcracks generated during the machining operation did weaken the sprayed ceramic structure making it more susceptible to the stresses induced during thermal shock testing. It is also possible that the results could have been affected by control of residual fabrication stresses.

Additional more complete property data generated under this program has identified a non-linear relationship between properties and temperatures. The sensitivity of property values with respect to temperature indicate the advisability of even more complete data to define the relationship even more accurately.

4.2 Recommendations

Testing (thermal shock, abradability and erosion) of the .045 inch thick ZrO_2 layer improved geometry system should be performed to substantiate the analytically expected improvements.

More complete definition of sprayed material properties is needed to more accurately predict performance of the ZrO_2/CoCrAlY seal system. The temperature dependence of the elastic and rupture modulii, in particular, should be substantiated by more testing at various intermediate temperature points. Possible changes in material properties and microstructure resulting from thermal exposure in an engine environment should also be investigated to evaluate the effect of aging on thermal shock characteristics of the seal system.

A study to determine the effects of machining the ZrO_2/CoCrAlY seal system and evaluate procedural changes to eliminate any adverse effects should be conducted.

Techniques for the control of fabrication stresses necessary for consistency and maximum life should be developed.